All Theses and Dissertations

2012-12-07

Liquid-Liquid Equilibrium of Biodiesel Components

Joseph C. Bell
Brigham Young University - Provo

Follow this and additional works at: https://scholarsarchive.byu.edu/etd

Part of the Chemical Engineering Commons

Liquid-Liquid Equilibrium of Biodiesel Components

Joseph C. Bell

A thesis submitted to the faculty of
Brigham Young University
in partial fulfillment of the requirements for the degree of

Master of Science

W. Vincent Wilding, Chair
Richard L. Rowley
Larry L. Baxter

Department of Chemical Engineering

Brigham Young University

December 2012

ABSTRACT

Liquid-Liquid Equilibrium of Biodiesel Components

Joseph C. Bell
Department of Chemical Engineering, BYU
Master of Science

Biodiesel is produced from vegetable oils through transesterification. Triglyceride mixtures extracted from oilseed feedstocks are upgraded by reaction with an alcohol in the presence of a catalyst to produce fatty acid esters. This reaction produces a mixture of esters, glycerin, alcohol, and catalyst. Separation of the fatty acid esters (biodiesel) and glycerin can be accomplished through liquid-liquid extraction by water addition. Designing liquid-liquid extraction with water as the solvent requires ternary liquid-liquid equilibrium data for mixtures of water, glycerin, and fatty acid esters. Ternary mixture LLE data have been experimentally measured for several of these systems. Those measured include mixtures with the methyl esters of lauric, myristic, palmitic, stearic, and oleic acids. Data were collected at atmospheric pressure and 60°C. These ternary systems have been correlated using the NRTL equation. These data and correlation parameters can be used to improve separations efficiency in trans-esterified biodiesel fuels.

ACKNOWLEDGMENTS

Table of Contents

List of Figures

List of Tables

Chapter 1   Introduction

The significance of energy in today's world cannot be adequately emphasized. Energy plays a vital role in everything we do. When one considers how many individuals participate, little things like turning on the lights, driving to work, or using a computer consume profuse amounts of energy. For example: U.S. energy consumption in 2008 was 99.3 quadrillion Btu[1]. This energy came from several sources; the largest being petroleum at 38%. The largest consumption sector was power generation at 40%, followed by transportation with 28%. Petroleum accounted for 95% of the total transportation energy, the remainder came from natural gas and renewable sources. This annual transportation energy need corresponds to approximately 250 billion gallons of gasoline, or about 2.2 gallons per person per day. This level of energy consumption is truly staggering.

An endless appetite for petroleum has many side effects on the environment, economy, and politics. The significance of these effects is currently a topic of debate. Among these side effects are notable effects on the environment and the large dependence on imports to satiate the ravenous national hunger for petroleum. The U.S. imports nearly 75% of the petroleum used[1], and this dependence on foreign oil

potentially jeopardizes national economic and political independence. These reasons,

and others, are sufficient to encourage development of alternative fuel sources.

1.1 Why Biofuels?

Biofuels are a plausible supplement to traditional fuels because they appear to

present solutions to many of the side effects of fossil fuels. While biofuels cannot

reasonably supply enough fuel to replace current fossil fuel consumption, the supply

they can produce should be pursued. Biofuels are renewable, and their use can

potentially decrease the environmental effects of current energy consumption levels. In

addition, biofuel use can help minimize dependence on foreign oil.

1.1.1 Renewability

Predictions regarding the duration of currently known oil reserves vary widely

in their time scales. However, independent of whom one chooses to believe, the

ultimate reality is that the petroleum on the planet is finite[2]. While the absolute amount

of petroleum is eventually limited, that of biofuels is not. They can be fully renewable;

a field of an oilseed crop can always be replanted. True renewability would also

requires the agricultural system to use only renewable energy sources, which it

currently does not. This renewability can have great effects on fuel consumption.

Biofuels are used as neat fuels (100% biofuel) and as mixtures with traditional fossil

fuels. Both of these strategies can substantially extend limited supplies of fossil fuels by

supplementing them with renewable biofuels.

1.1.2 Environmental Impacts

Fossil fuels used as motor fuels are hydrocarbon mixtures containing little or no oxygen. Biofuels, however, are oxygenated fuels.   When biofuels are burned the oxygen already in the fuel effectively alters the air/fuel ratio. This affects the combustion chemistry and products and changes the tailpipe emissions. Higher oxygen-to-fuel ratios in biofuels tend to appreciably decrease carbon monoxide and hydrocarbon emissions, often by as much as 50%[3-4]. An emission comparison of other pollutants is less clear, specifically when considering NO_x. While some authors indicate that biofuels have lower NO_x emissions[3], most authors show that biofuels actually have slightly higher NO_x emissions than fossil fuels[4-6].

Biofuels exhibit relatively low lifecycle CO_2 emissions. While some authors may indicate slight changes in tailpipe CO_2 emissions for biofuels over traditional fossil fuels, in general there is very little change in CO_2 emissions per mile driven for the two fuels[7]. The real CO_2 benefit of biofuels comes from a lifecycle analysis: including CO_2 absorbed by crops grown to produce biofuel. When plant-absorbed CO_2 is included in analyses, net emissions of CO_2 can be reduced by up to 78% compared to petroleum fuels. This dramatic decrease in net CO_2 emissions is of prime interest in reducing greenhouse gas emissions[2].

1.1.3 Political / Economic Impacts

As mentioned previously, the U.S. imports nearly 75% of the petroleum consumed nationally. This represents significant economic out flux to other nations. It also removes a certain amount of national independence by placing the U.S. at the mercy, so to speak, of the countries who export oil. Biofuels have the potential of re-directing some of the dollars currently spent on oil importing to local farmers and producers of biofuels. Accompanying this economic shift would also be a shift towards increased levels of national independence by relying less on oil exporting nations to meet domestic energy needs[2].

These several points attract attention to biofuels. They are potentially 100% renewable, and current research and analyses indicate that biofuels impact the environment less than traditional fossil fuels. Additionally, they can decrease some of the negative political and economic side effects of importing vast amounts of foreign petroleum. Biofuels can play a significant role in the solution to the ever increasing transportation energy crisis[8].

Chapter 2   Literature Review

Biomass can be converted to a more convenient energy source through several pathways. Each pathway provides different forms of energy including gases, liquids, solids, or simply heat. Transportation energy needs demand a liquid fuel because of its high energy density and because it is easy to transport, store, and use. Of the various possible pathways for converting biomass to more usable energy forms, three directly produce a liquid fuel product. These include pyrolysis with a bio-oil product, biological fermentation producing ethanol, and mechanical or chemical oil extraction to produce vegetable oils which are then upgraded to biodiesel. For all of these biofuels there are various considerations regarding production and use, these include: different feedstocks, distinct processing, and fuels with unique characteristics. While the focus of this work will be on biodiesel, each of these considerations will be briefly discussed for all three types of liquid biofuel.

There are additional processes requiring multiple conversion steps which can be used for converting solid bio material into a liquid fuel. An example is gasification to produce a syngas which is then used in a Fischer-Tropsch process to produce high-quality, sulfur free diesel fuel. This may be the most prevalent process for producing

transport fuels from solids in the absence of subsidies, however it will not be

investigated here.

2.1 Pyrolysis – Bio-oils

Pyrolysis is thermal decomposition in an oxygen deficient atmosphere. Pyrolysis

can produce a gaseous, liquid, or solid char product and most commonly produces a

combination of all three. Process variables such as reactor residence time and

temperature control the amount of each product obtained. Long residence times and

high temperatures favor gas production, while long residence times and low

temperatures favor char production. Very short residence times at moderate

temperatures tend to produce high amounts of liquids. This is referred to as "fast

pyrolysis" because of the short residence times, usually 1-2 seconds or less[9].

Ideally pyrolysis of any form of biomass can produce a liquid fuel. While some

biomass may produce more liquids, such as wood chips, and others may produce

significantly less liquid and more gas, such as grasses, any biomass can be used.

Biomass residues from farming or food production and forest residues are attractive

biomass sources as they are currently discarded as waste, often at a substantial expense,

and are readily available[10].

2.1.1 Process Specifics

Fast pyrolysis consists of rapidly heating biomass to a controlled moderate temperature. For maximum liquid production, the temperature should be around 500 °C, depending on feedstock and other factors. The biomass decomposes to generate mostly vapors and aerosols. These must be quickly quenched, within 1-2 seconds, to produce the bio-oil product[11].

The very rapid heating required for the decomposition to produce the desired range of products necessitates special treatment of the biomass feed and the reactor system. Biomass must be finely ground to around a 2mm particle size, and dried to a water content of <10% for the high heat transfer to be effective. Special attention must also be given to the reactor designed to accomplish high heat transfer rates and short residence times. A wide variety of reactors has been studied on small lab scales. These include bubbling fluidized beds, circulating fluidized beds, high pressure vortices, spinning plates, and rotating cones. While all of these methods have been successfully demonstrated on laboratory scales, scaling them up to industrial levels presents significant problems with maintaining the necessary heat transfer rates[9-11]. Despite these difficulties, several industrial scale operations do exist. Honeywell has a daughter company called Envergent Technologies, producing pyrolysis oil with a circulating fluidized bed[12]. Another company called BTG-BTL has an industrial process based on the rotating cone reactor[13].

2.1.2 Products

The bio-oil produced by fast pyrolysis is a viscous, acidic, highly oxygenated, chemically complex and relatively unstable mixture containing both suspended solids and inorganic component in far higher concentrations than any typical liquid fuel. The oil may contain more than 300 different compounds, making it difficult to characterize and/or purify. Typical pyrolysis oil contains up to 25% water and is not compatible with traditional transportation fuels. Significant upgrading is required to use bio-oils attainable by current pyrolysis technology as transportation fuels[10-11, 14].

While pyrolysis oils are very complex mixtures of hundreds of compounds making them difficult to characterize and separate, many of the individual compounds contained in pyrolysis oils have already been extensively studied and are well understood. The majority of the compounds that have been identified in pyrolysis oils are light aromatic, oxygenated, and aliphatic compounds. Table 1 shows a list of some of the compounds identified in pyrolysis bio-oils by several investigators. The compounds underlined in Table 1 are compounds that are also included in the DIPPR® 801 database and are already well characterized.

Table 1: Partial list of compounds found in pyrolysis bio-oils[10-11]

Aromatic and polycyclic aromatic compounds

Benzene	Methylnaphthalenes	Phenanthrene
Toluene	Dimethylnaphthalenes	Methylphenanthrenes
Ethylbenzene	Trimethylnapthalenes	Dimethylphenanthrenes
Dimethylbenzenes	Tetramethylnaphthalenes	Trimethylphenanthrenes
Trimethylbenzenes	Fluorene	Tetramethylphenanthrene
Tetramethylbenzene	Methylfluorene	Pyrene
Benzofuran	Methylfluoranthene	Methylpyrene
Methylbenzofuran	Anthracene	Benzo[a]pyrene
Naphthalene	Chrysene	Benzo[e]pyrene

Oxygenated Compounds

Acetic acid methyl ester	Methoxyphenol	Phenol
Acetic acid propyl ester	Dimethylphenols	Benzenediol
2-Cyclopentan-1-one	Ethoxyphenol	Methylfuranone
Methylcyclopentanone	Methylbenzenediols	Methylphenols
Furanone	Trimethylphenols	Methylnaphthenols
Dimethoxypropenylphenols	Methoxypropenylphenol	Dimethylnaphthenols
Naphthenols	2-Hydroxy-3-methylcyclopentanone	Methyl furfural

Aliphatic Compounds

Methane	Ethane	Ethylene
Acetylene	Propane	Propylene

Reference [11] states that as much as 14.3% of the pyrolysis oil was found to be aliphatic compounds, however further characterization than that listed here is not provided

2.2 Biological Fermentation – Ethanol Production

Most of the world's ethanol is produced through microbial conversion of biomass feedstocks through a fermentation process. The micro-organisms used for the fermentation can usually feed on any 6 carbon sugar, commonly glucose, and sometimes 5 carbon sugars. While almost any fungus, bacteria, or yeast, can be used for fermentation the most frequently used to ferment glucose is *saccharomyces cerevisiae*; the same yeast commonly used in the baking industry[15].

Any biomass containing high levels of glucose in any form can be a potential

source for ethanol production. One group of potential feedstocks is actual sugar crops,

such as sugarcane, sugar beets or various fruits. The sugar in these sources is readily

available for yeast consumption, making the process relatively efficient. Brazil has a

very successful national program producing ethanol from sugarcane. Considering

these sugar crops are all in the human food chain they are commonly cultivated but are

also expensive. This presents a drawback to using them as fuel sources[15-16].

A second group of biomaterials that have been used for ethanol production are

starchy sources. Starches are long chains of glucose molecules joined by α-linkages

producing a non-linear polymer. Starches can be broken into individual glucose

molecules, by hydrolysis with heat and water, which can then be consumed by yeast.

Commonly used starch sources for ethanol production include potatoes, wheat, and

corn. These sources are also all in the human food chain, and are consequently

expensive[15].

In both the plant sugars and the starchy sources, the amount of plant material

that can be converted to ethanol is very small compared to the bulk of the plant. The

great majority of all plant matter consists of cellulose, hemicellulose, and lignin, which

comprise the third group of potential sources. Cellulose is also a polymer of glucose.

However, unlike non-linear starches, cellulose is a linear polymer of glucose molecules

joined by β-linkages.   Linear cellulose molecules are typically aligned parallel to each

other and extensively joined together by hydrogen bonding making cellulose more

difficult to hydrolyze than starches. These materials typically consist of about ⅓

cellulose, ⅓ hemicellulose (a polymer of glucose and xylose), and ⅓ lignin. Lignin

surrounds the cellulose and contains no sugar, and therefore cannot be converted into

ethanol by yeast. Cellulosic materials include paper, cardboard, wood and other forest

wastes, or any other fibrous plant material. Many of these materials are considered

waste, and none are in the human food chain. Because of this, they can be less

expensive feedstocks to use[16].

2.2.1   Process Specifics

The pre-treatments required before fermentation vary based on the feedstock.

Cellulosic biomass requires the most complex pretreatment. Cellulosic biomass must

first be physically reduced to a size compatible with later processes.   This can be

accomplished by chipping, grinding, or any other adequate size reduction method.

Following size reduction the biomass is treated with an organic solvent, usually at high

temperature, to disrupt the lignin complex and expose the cellulose and hemicellulose.

The next step is hydrolysis, where the long chain polymers are broken down into

individual sugars. Starchy feedstocks begin their processing at this stage. Hydrolysis

can be performed either by enzymes, acid hydrolysis, or in the case of starches, with

heat and water. The hydrolysis process produces a glucose-rich syrup ready for

fermentation[17].

The final step in biological ethanol production from any feedstock is

fermentation. While there are many variations for carrying out the fermentation of

glucose to ethanol, they all follow the same general course. The micro-organisms of

choice are added to the post-hydrolysis syrup, and appropriate temperature and pH

conditions are maintained for the organisms to flourish. During fermentation the

organisms use some of the energy contained in the glucose to support life functions and

reproduce, while converting much of the glucose into ethanol, a by-product of their

growth[16-17].

2.2.2   Products and Separations

The solution after fermentation is a complex mixture that may contain biomass

pieces in various stages of decomposition, cellulose, lignin, un-digested sugars, yeast,

acid or base, CO_2, water, and about 5% ethanol. Simple distillation yields concentrated

ethanol at the ethanol-water azeotrope (≈95 wt% ethanol), a system that is already well

characterized with extensive experimental data. The remainder of the mixture is then

returned to the fermentation stage, or discarded as waste. If higher concentrations of

ethanol are required it must be further purified by distillation with an entrainer or by

pressure swing distillation to break the azeotrope and produce pure ethanol[16].

2.3 Oil Extraction and Upgrading – Biodiesel Production

Biodiesel is produced from vegetable oils through an organic reaction. Many vegetable oils are quickly and efficiently produced on a large scale for human consumption. Because of this ready availability oils like canola, corn, palm, and soybean have been investigated for biodiesel production[18-19]. However, as with ethanol feedstocks these oils can be expensive because they are grown for human consumption[15].

This expense has led to interest in alternate vegetable oil sources not in the human food chain: like linseed and rapeseed oils[4]. Smaller scale oil sources have also been investigated; these include used cooking oils, animal fats, and less common food oils[20-21]. Another attractive potential source is algae oils as they do not require arable farmland nor are they in the human food supply. Algae grow quickly and easily in fresh and salt water environments, and can have high oil productivity[22-23]. While each of these oil sources produces biodiesel with a different distribution of compounds, similar processes are used to produce biodiesel from all the oils.

2.3.1 Reaction Specifics and Chemistry

Biodiesel is produced from vegetable oil through transesterification, an organic reaction where one ester is transformed into a different ester. In vegetable oil transesterification, a triglyceride is reacted with an alcohol in the presence of a catalyst to produce glycerin and fatty acid alkyl esters[24-25]. This is represented in Figure 1. Most

13

investigators have selected methanol or ethanol as the alcohol of choice due to low costs

and high availability. While stoichiometry dictates a molar alcohol to triglyceride ratio

of 3:1, excess alcohol is generally used to increase yield and to aid in separation. A

variety of catalysts can be used; each catalyst requiring different conditions and

providing unique advantages.
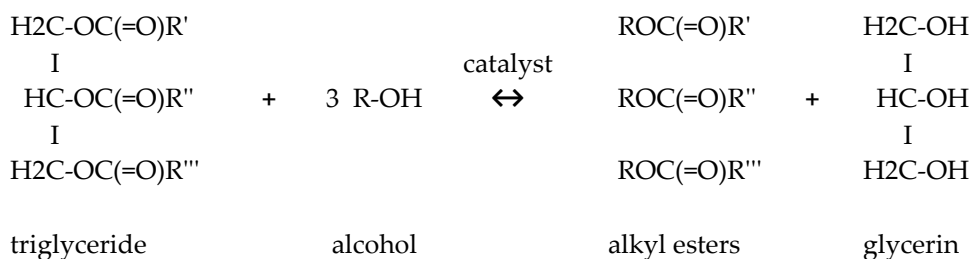
```
H2C-OC(=O)R'                                      ROC(=O)R'        H2C-OH
 I                                  catalyst                         I
 HC-OC(=O)R"      +     3 R-OH        ↔           ROC(=O)R"    +    HC-OH
 I                                                                  I
H2C-OC(=O)R'''                                    ROC(=O)R'''      H2C-OH

triglyceride              alcohol              alkyl esters        glycerin
```
Figure 1: Transesterification of vegetable oils

The process can by catalyzed by a Brønsted acid, such as sulfonic or sulfuric acid.

Acid catalysts frequently require more than 3 hours and temperatures in excess of 100

°C to attain complete conversion[26]. Reaction time for conversion increases with smaller

alcohols. For example, methanolysis of soybean oil at an alcohol/oil molar ratio of 30:1

takes 50 hours, while reaction with ethanol in the same ratio requires only 18 hours. An

advantage of the acid catalyzed reaction is that it does eventually reach complete

conversion (>99%) of the vegetable oil[25].

Alternatively the process can be catalyzed by bases. Because these catalysts are

less corrosive and the reactions proceed much faster they tend to be favored. Alkaline

metal alkoxides, like CH_3ONa, make good basic catalysts because they provide for very

high conversion (>98%) in shorter periods of time (30 min) and at low concentrations (0.5 mol%)[19, 26]. Drawbacks of these catalysts are that they require the complete absence of water, and they are expensive. A significantly cheaper alternative is the use of alkaline metal hydroxides, such as KOH and NaOH, but they are also less active. The lower cost offsets the need to use more because of lower activity and catalyst deactivation that may occur due to the presence of water. These catalysts have been shown to be effective with alcohol/oil molar ratios of 6:1[26]. With a moderate temperature of 60 °C and a catalyst concentration of 1 mol% they provide the same conversion (≈98%) on a similar time scale (30-90 min) as alkoxide catalysts[18].

Various other catalysts have been investigated for transesterification of triglycerides, though not as extensively as acid and base catalysts. These include lipase catalysts and non-ionic basic catalysts that are frequently used in organic synthesis, as well as heterogeneous catalysts of organic bases on organic polymers. None of these produces the high yields and short reaction times attainable with ionic basic catalysts[24].

2.3.2   Products and Separations

The transesterification reaction produces a mixture of various fatty acid esters, glycerin, alcohol, water, and catalyst. As illustrated previously in Figure 1 the R group of the ester is determined by the alcohol used. The R', R'', and R''' groups are determined by the parent triglycerides. Each vegetable oil source has a different composition of triglycerides, and therefore will produce a unique mixture of fatty acid

esters. Table 2 shows the fatty acid compositions of various vegetable oils that have drawn some attention as biodiesel sources, and consequently the fatty acid ester compositions of biodiesel produced from these oils.

After transesterification it is necessary to separate the fatty acid ester from the alcohol and glycerin, along with the catalyst and any water that may be present. Nearly all of the alcohol (≈94%) can be immediately recovered by distillation. This may require vacuum distillation to maintain the bottoms temperature below about 150 °C, above which both the fatty acid esters and glycerin begin to decompose[20].

Table 2: Fatty acid composition of various oils[21, 27]

	Weight Percent Fatty Acid Composition													
Chain Length	8	10	12	14	16	18	20	22	24	18	18	22	18	18
Double Bonds	0	0	0	0	0	0	0	0	0	1	1	1	2	3
Vegetable Oil	Caprylic	Capric	Lauric	Myristic	Palmitic	Stearic	Arachedic	Behenic	Lignoceric	Oleic	Ricinoleic	Erucic	Linoleic	α-Linolenic
Beef tallow	-	0.1	0.1	3.3	25.2	19.2	-	-	-	48.9	-	-	2.7	0.5
Canola	-	-	-	0.1	3.9	3.1	-	-	-	60.2	-	0.5	21.1	11.1
Castor	-	-	-	-	1.1	3.1	-	-	-	4.9	89.6	-	1.3	-
Coconut	8.3	6.0	46.7	18.3	9.2	2.9	-	-	-	6.9	-	-	1.7	-
Corn	-	-	-	-	11.7	1.9	0.2	-	-	25.2	-	-	60.6	0.5
Cottonseed	-	-	-	-	28.3	0.9	-	-	-	13.3	-	-	57.5	-
Crambe	-	-	-	-	2.1	0.7	2.1	0.8	1.1	18.9	-	58.5	9.0	6.9
Linseed	-	-	-	-	4.9	2.4	-	-	-	19.7	-	-	18.0	54.9
Palm	0.1	0.1	0.9	1.3	43.9	4.9	-	-	-	39.0	-	-	9.5	0.3
Palm kernel	2.5	4.0	48.2	16.2	8.4	3.0	-	-	-	15.3	-	-	2.3	-
Peanut	-	-	-	-	11.4	2.4	1.3	2.5	1.2	48.3	-	-	32.0	0.9
Rapeseed	-	-	-	-	2.7	2.8	-	-	-	21.9	-	50.9	13.1	8.6
Rice Bran	-	-	-	0.3	17.2	1.7	1.2	-	-	45.8	-	-	33.4	0.4
Safflower	-	-	-	-	8.6	1.9	-	-	-	11.6	-	-	77.9	-
HO Safflower	-	-	-	0.3	5.5	1.8	0.2	-	-	79.4	-	-	12.9	-
Sesame	-	-	-	-	13.1	3.9	-	-	-	52.8	-	-	30.1	-
Soybean	-	-	-	-	11.8	3.2	-	-	-	23.3	-	-	55.5	6.3
Sunflower	-	-	-	-	6.1	3.3	-	-	-	16.9	-	-	73.7	-

Two methods have been suggested to accomplish the separation of the fatty acid

esters and glycerin. One method is separation by gravity settling and phase

separation[28-29]. This requires space and time and is therefore not an optimal industrial

method. The other method is through liquid-liquid extraction by solvent addition,

generally water[20, 30-31]. In both methods the fatty acid ester and glycerin phases must be

further purified to obtain high purity products. This purification step can again be

accomplished through vacuum distillation, producing pure fatty acid esters (biodiesel)

and glycerin, as well as streams of mixed alcohol and water which can be recycled or

treated as waste[20].

2.4 Biodiesel Thermophysical Properties

Each separation process previously mentioned in the purification of biodiesel

cannot be truly optimized without accurate fundamental properties. The separation of

alcohol from the reaction products by distillation necessitates accurate vapor-liquid

equilibrium data for mixtures of fatty acid esters and alcohols. Designing liquid-liquid

extraction with water as the solvent requires liquid-liquid equilibrium (LLE) data with

water and glycerin. These accurate thermophysical property data for all system

components are essential for efficient process design.

Based on information shown in Table 2, a set of esters of the most commonly

occurring fatty acids would be representative of the range of products obtained from

17

potential biodiesel feedstocks. Because methanol and ethanol appear to be the most

common alcohols for biodiesel production, due to low cost and high availability, a

sufficient starting point for a database of biodiesel LLE properties is with methyl and

ethyl esters of the most common fatty acids. Table 3 shows these esters of the most

common fatty acids, where R represents either a methyl or ethyl group.

Table 3: Esters of the most common fatty acids

Methyl Ester	Ethyl Ester	Fatty Acid	Chemical Structure
$C_{13}H_{26}O_2$	$C_{14}H_{28}O_2$	Laurate	
$C_{15}H_{30}O_2$	$C_{16}H_{32}O_2$	Myristate	
$C_{17}H_{34}O_2$	$C_{18}H_{36}O_2$	Palmitate	
$C_{19}H_{38}O_2$	$C_{20}H_{40}O_2$	Stearate	
$C_{19}H_{36}O_2$	$C_{20}H_{38}O_2$	Oleate	
$C_{19}H_{34}O_2$	$C_{20}H_{36}O_2$	Linoleate	
$C_{19}H_{32}O_2$	$C_{20}H_{34}O_2$	Linolenate	
$C_{23}H_{44}O_2$	$C_{24}H_{46}O_2$	Erucate	

R- Represents CH_3 or C_2H_5 for the methyl and ethyl ester, respectively.

Literature searches have returned very little vapor-liquid equilibrium data for

these fatty acid esters with their parent alcohols. One author measured data for systems

of methyl laurate and methyl myristate with methanol, as well as ethyl laurate and

ethyl myristate with ethanol[32-33]. However, these data are subject to question because

the temperature at which they were measured is very near the ester's decomposition

temperature[34]. Literature vapor-liquid equilibrium data for mixtures of these esters

with their parent triglycerides are also non-existent. In the event of incomplete

conversion in the reaction, these data are necessary to efficiently separate the biodiesel

product from un-reacted vegetable oil.

Literature searches have returned little information regarding the LLE of fatty-

acid esters with glycerin and water. Perhaps the most vital separation step in biodiesel

production is separating the desired fatty-acid methyl ester product from the glycerin

by-product. This separations step cannot be optimized without accurate data. These

data are not found in the literature. Several investigators have studied LLE in mixtures

of a fatty-acid methyl ester, glycerin, and methanol[35-36]. However, at the liquid-liquid

extraction stage of the process, almost all the methanol has already been removed, and

water is added to aid in the separation. Two different investigators discuss attempts at

modeling this LLE behavior in mixtures of fatty-acid methyl ester, glycerin, and water,

and state that accurate experimental data are needed[20, 31].

The current level of experimental data for these biodiesel compounds and

mixtures has been inadequate for effective optimization of process designs. If biodiesel

use is expected to replace a portion of current petroleum consumption, further work to

obtain essential data is necessary. These data must include LLE of fatty acid esters with

water and glycerin. Accurate data should prove to be significant in improving biodiesel

19

process economics and can enable biodiesel to become a more mainstream

transportation fuel source.

Chapter 3   Objectives

The overall goal of this research is to provide important thermophysical property data for biodiesel components which will be of process design interest for biodiesel production processes. The property of interest is ternary mixture LLE data for the components listed in Table 3 with glycerin and water.

The first objective was to obtain existing published data for the previously stated LLE systems and evaluate these data for thermodynamic consistency and accuracy. After thorough literature searches no published LLE data were located for any of these systems. Based on this evaluation the second and primary objective was to provide experimental data for the previously mentioned ternary LLE systems.

Table 4 shows the availability and purity of each of the components listed in Table 3. The focus of the experimental work was to measure LLE data for each of the ten available components listed in Table 4 with glycerin and water. The experimental temperature and pressure were 60° C and atmospheric pressure. These choices of temperature and pressure were based on process design models by Zhang[20]. Due to time constraints, measurements with the ethyl esters were omitted. Measurements with

the methyl esters included binodal and tie line data. The following sections describe the

LLE measurements made during this study and the results obtained.

Table 4: Availability and purity of components shown in Table 3

Component	Availability / Purity	Component	Availability / Purity
Methyl laurate	>98%	Ethyl laurate	>98%
Methyl myristate	>98%	Ethyl myristate	>98%
Methyl palmitate	>97%	Ethyl palmitate	>95%
Methyl stearate	>96%	Ethyl stearate	>97%
Methyl oleate	>99%	Ethyl oleate	>70%
Methyl linoleate	Not available	Ethyl linoleate	Not Available
Methyl linolenate	Not available	Ethyl linolenate	Not Available
Methyl erucate	Not available	Ethyl erucate	Not Available

Chapter 4   Experimental Measurements

There are several prominent methods for measuring ternary LLE data. A

commonly used method for measuring the binodal curve is cloud point titration[37]. A

known mixture of two components is titrated with the third until the cloud point is

reached, indicating the formation of a second phase. The cloud point may be defined

visually by the appearance of cloudiness[38] or by scattered light intensity from a light

source and sensor[39-40].

The initial direction of this work was to measure the binodal curve by cloud

point titration; however, attempts at performing titrations with the desired mixtures

quickly showed this method was impractical. The relatively coarse increments in which

titrant can be added were too large for the systems being investigated. This coarseness

makes the cloud point difficult to observe in systems where the two phases exhibit very

low mutual solubility making it a poor method choice in this situation.

Because of this difficulty the binodal curve and tie lines were measured by GC

analysis. A mixture in the two phase region containing known amounts of three

components was thoroughly mixed and allowed to separate and equilibrate. After an

allotted time had passed both phases were sampled and compositions analyzed by

GC[41-43] and Karl Fischer titration. This simultaneously provided the binodal curve and tie lines throughout the two phase region. Details of the experimental apparatus and methods, as well as the analytical and statistical methods are outlined here. An extended discussion of method and apparatus development is included in Appendix B.

4.1 Experimental Apparatus

Equilibrium experiments were carried out in a custom made cylindrical glass cell (Figure 2-B) obtained from Ace Glass. The volume of the cell was approximately 250mL. The top of the cell was threaded with coarse threads to receive a matching PTFE cap (not pictured), fitted with an O-ring to seal the vessel. The cap was machined with five holes passing through, and in each hole was inserted a threaded stainless steel fitting.

Two of these fittings contained sampling lines (Figure 2-F) with tubing extending into each of the two liquid phases. Sampling lines were 1/16 in stainless steel tubing with HIP valves attached to stainless steel Luer-Lok syringe ports. Samples were extracted through these lines directly into a syringe with no need for a needle or septum. A third fitting in the cap contained a thermo-well for measurement of the actual temperature in the mixture via an inserted Omega PR-13-2-100 RTD (Figure 2-G). A fourth fitting connected to tubing (not pictured) allowed the vapor space in the cell to be pressurized with nitrogen, evacuated by vacuum, or vented to the atmosphere.
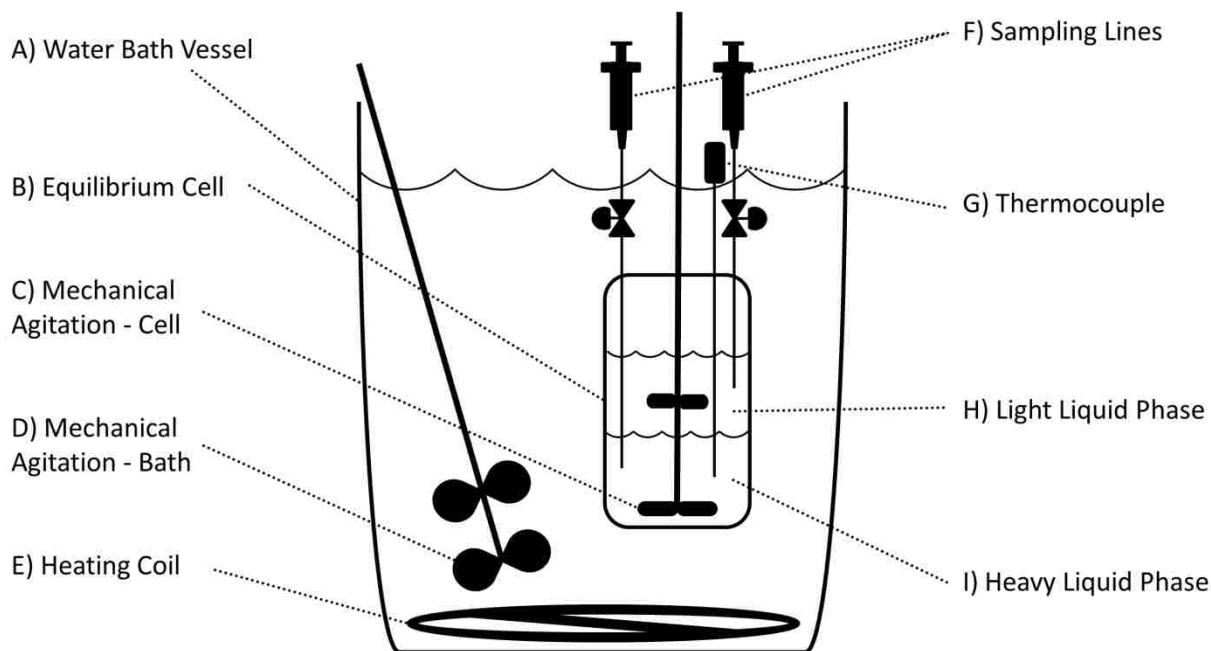
Figure 2: Experimental apparatus

A custom made compression fitting allowed a stir shaft (Figure 2-C) to pass through the center of the cap, sealing the shaft with two compressed O-rings. These O-rings were lubricated with Krytox® synthetic lubricant to maintain a seal with the shaft spinning, and to extend the life of the O-rings. The shaft was fitted with two propellers, one positioned in each of the liquid phases, to provide adequate stirring in each phase and ensure intimate contact of the two phases. Stirring was accomplished with a Servodyne SSM52, high-torque low-RPM stirrer (not pictured). This stirrer maintains a specific RPM by adjusting the torque as necessary to overcome friction from the compression seal in the PTFE cap as well as from the viscous mixture in the cell.

The glass cell was held in place with a pair of ring clamps to prevent it from moving or spinning during stirring (not pictured). This entire equilibrium cell and

support structure was contained within a temperature controlled water bath (Figure 2-A). Temperature control was provided by an Omega CS2110 temperature controller, with an Omega PR-13-2-100 RTD in the bath and a 1500 W resistance heating coil submerged in the bath (Figure 2-E). Thorough mixing of the water bath was provided by a Talboys model 107 stirrer (1500 RPM) with two, three inch propellers (Figure 2-D). This provided for temperature control inside the cell to within ±0.1 K of the set point.

The temperature at which experiments were performed (60°C) provided for a relatively high evaporation rate from the water bath. To combat this, the water level in the bath was maintained by a float valve (not pictured) gravity fed from a secondary tank. Additionally, the surface of the water was covered with packing peanuts (not pictured) to slow the evaporation rate.

4.2 Experimental Methods

4.2.1 Chemical Supplies

Deionized and distilled water as plumbed through the chemistry building was used for the equilibrium experiments. The water was used directly from the source with no further purification. All other chemicals used were obtained from Sigma-Aldrich. While each chemical came from the supplier with a lot analysis, the purity of each chemical was also verified by GC analysis. Chemicals were all used as received,

with no further treatment. Table 5 shows the actual purities of the chemicals used in

the equilibrium experiments.

<div align="center">Table 5: Purity of chemicals used</div>

Component	Actual Purity
Methyl caprate (internal standard)	99.3%
Methyl laurate	99.1%
Methyl myristate	99.9%
Methyl palmitate	99.0%
Methyl stearate	98.7%
Methyl oleate	99.6%
Glycerin	99.9%

4.2.2 Buoyancy Corrections

Addition or subtraction of a component to or from a vessel changes the volume

of air displaced by the vessel and its contents. Because objects in air experience a

supporting buoyant force proportional to the volume of air displaced, a change in

volume will be accompanied by a change in this buoyant force. Any comparison of

masses of differing volumes must be corrected to account for this change in buoyancy[44].

Throughout the experimental methods that follow the mass of a component or sample

was determined by taking a difference in mass before and after the addition (or

subtraction) of the component to or from a vessel. The buoyancy corrected mass (M_{BC})

was determined according to Equation 1.

$$M_{BC} = abs\left(M_{final} - M_{initial} + \left(V_{final} - V_{initial}\right)\rho_{air}\right) \tag{1}$$

The second half of Equation 1 represents the buoyancy correction. Here V_{final} and $V_{initial}$ refer to the total volume of a vessel and all its contents. Similarly M_{final} and $M_{initial}$ refer to the total mass of a vessel and its contents. In practice the total volume of a vessel and its contents was never determined. Instead the change in volume was assumed to be equal to the volume added (or removed). The density of air (ρ_{air}) was found using the ideal gas law as shown in Equation 2. This calculation made use of the ambient temperature (T) and pressure (P) at the time of measurement and the gas constant (R_g). The average molecular weight of air (MW_{air}) was assumed to be 28.84 gm/mol. On average the buoyancy correction was approximately 1 mg/mL.

$$\rho_{air} = \frac{P}{R_g T} MW_{air} \qquad (2)$$

4.2.3 Charging the Cell

The cell was charged with a ternary mixture of water, glycerin, and a fatty-acid methyl ester. The initial composition of the cell was determined by specifying an overall water content of the mixture. The amount of each component to add was then calculated such that there were approximately 60 mL of each phase in the cell. This provided an adequate amount of each phase for sampling, while maintaining the total liquid volume in the cell as small as possible to ensure thorough mixing.

After an appropriate amount of each component was added, the cell was fastened in place within the water bath. The vapor space above the liquid mixture was

purged by first pressurizing the cell with nitrogen (provided by AirGas at 99.998%) to approximately 20 psia, followed by evacuating the cell to approximately 1 psia. This cycle was repeated three times. On the third cycle instead of evacuating by vacuum, the cell was vented to the atmosphere. The vent valve remained slightly open after releasing excess nitrogen pressure. This limited vapor space communication with the atmosphere while maintaining ambient pressure in the cell throughout the heating, stirring, and settling stages.

Adequate time was allowed for the water bath and cell to reach the set point temperature of 60° C. During this time the cell was slowly stirred to facilitate heat transfer. When the temperature had equilibrated, the mixture was stirred at 700 RPM for 30 min. This stirring rate provided intimate mixing of the two phases. By the end of the allotted stirring time the mixture was an even emulsion. In most cases individual bubbles of each phase were not visible; instead the mixture was cloudy throughout.

This cloudy mixture was left to settle long enough for the two phases to fully disengage. Experiments investigating the effects of settling time ranged from a few hours to several weeks. The results indicated that once both phases returned to a completely clear state, especially near the meniscus between the two liquids, there would be no further changes in composition. While a few experiments required a

somewhat longer settling time, in most cases two clear phases were obtained within 24 hours.

4.2.4 Equilibrium Sample Extraction

Following the required settling time and immediately prior to extracting samples, the sampling line for each phase was purged. Approximately 5 mL of a phase was extracted through the line and discarded as waste. This volume corresponds to about 30 times the dead volume of the sampling line and valve.

Because the composition analysis consisted of two distinct destructive analyses, two sets of samples were required. First a 0.8 mL sample was extracted followed by a sample ranging in size from 0.1 to 3 mL. The 0.8 mL sample was later prepared for GC analysis where glycerin and methyl ester content were determined, while the second sample was for water analysis. Five more similar pairs of samples were extracted, for a total of 6 GC samples and 6 water analysis samples from each phase.

The water analysis sample size for the light (methyl ester) phase was always 3 mL. Water analysis sample sizes for the heavy (glycerin/water) phase ranged from 0.1 to 1 mL depending on the water content of the charge. Smaller sample sizes were used with higher water content charges, keeping the time required for titration at a reasonable level.

Throughout the purge and sample processes the inlets of the sampling lines were visually observed to ensure that they were in the appropriate phase and sufficiently far from the meniscus or bubbles of the opposing phase. Occasionally there were small bubbles of the opposing phase adhered to the outside of the sampling line, or the walls of the glass cell. In the event that one of these bubbles entered the line the sample in question was discarded. The sampling line was then re-purged as previously described and sampling resumed.

4.2.5 Analytical Sample Preparation

Prior to GC analysis, the extracted equilibrium samples were diluted in methanol to avoid saturating the GC column with methyl esters and glycerin. Methyl caprate was also added as an internal standard to assist in quantifying components and reduce instrument variability[45-46]. Glass vials with rubber septa were labeled and weighed. A constant volume of internal standard (0.2 mL) was added to each vial and the vials weighed. Subsequently 4 mL of methanol were added and the vials were again weighed. Finally one 0.8 mL sample extracted from the equilibrium cell was added to each vial, and a final mass recorded. The masses of methanol ($M_{methanol}$), internal standard (M_{ISTD}), and equilibrium sample ($M_{equ\,sam}$) in the analytical sample were taken as the differences between the before and after masses, corrected for buoyancy effects.

The mass fraction[§] of equilibrium sample in the prepared analytical sample $\left(MF_{equ\ sam}^{(a)}\right)$ was calculated according to Equation 3 for later use. The mass fraction of internal standard was also calculated in a similar manner.

$$MF_{equ\ sam}^{(a)} = \frac{M_{equ\ sam}}{M_{equ\ sam} + M_{ISTD} + M_{methanol}}$$ (3)

After thorough mixing, a small quantity (1-1.5mL) of this prepared analytical sample was extracted and placed in a small 2mL vial designed for use with the GC auto-sampler. Once the auto-sampler vials' septa had been punctured during analysis, the methanol slowly escaped at a rate of a few mg per day. This rendered the auto-sampler vials useless for any further analysis more than a few hours after the initial analysis. The vials containing the original analytical sample preparation were therefore tightly capped and stored in the event they were needed for future analyses.

After all samples had been extracted and prepared, any remaining phases in the equilibrium cell were discarded as waste. The cell and sampling lines were thoroughly washed with soapy water, rinsed with acetone, and dried with flowing nitrogen prior to the next charge.

[§] The notation for mass fractions included hereafter is as follows: the superscript *(a)* refers to a mass fraction in a prepared analytical sample, the superscript *(s)* indicates a mass fraction in a prepared standard solution, and no superscript refers to a mass fraction in an equilibrium sample.

4.2.6   Calibration Standard Preparation

Calibration standards were prepared by making a series of dilutions of the component of interest, either glycerin or a methyl ester, in methanol. The dilutions were performed in glass vials with rubber septa. The actual masses of components added were taken as the difference of an initial and final mass, corrected for buoyancy.

Starting with a pure methyl ester, a dilution containing 10 %wt of the pure component with the balance methanol was prepared. A second dilution containing 10 %wt of the first dilution, balance methanol, was then prepared. This was repeated four more times with each consecutive dilution being prepared from the previous dilution. This resulted in a total of 7 concentrations, the pure component plus six dilutions. Concentrations included in the ester calibration series by this method range from mass fractions of 1 to 1×10^{-6}.

Calibration standards for glycerin were prepared in a similar fashion; however, after the first dilution to 10 %wt the remaining dilutions were by a factor of 5 instead of 10. That is, they were diluted to 20 %wt of the previous dilution, with the balance methanol. This was done to increase the number of calibration points before the concentration dropped below the detection limit. This provided for a series of standards ranging from mass fractions of 1 to 3.2×10^{-5}. This is well below the ASTM limits for glycerin in neat biodiesel[31].

Each of these standard solutions was then prepared for GC analysis in the same way as the samples extracted from the equilibrium cell, as previously described. A volume of 0.8 mL of the standard solution was added to a known mixture of methanol and internal standard, mixed, and a small sample extracted for analysis. These samples were then analyzed by GC according to the same methods used for analyzing the equilibrium samples, which method will be described hereafter.

4.3   Analytical and Statistical Methods

Attempts were made at developing an analytical method requiring a single analysis to determine compositions of all three components. None of these methods provided the desired precision and accuracy; therefore, the analysis was performed in two distinct steps. As was previously stated, two sets of samples were taken from each equilibrium phase. One set was used to determine water content by Karl Fischer titration, while the other was used to establish methyl ester and glycerin concentration via GC analysis. Concentrations of the two minor components were determined experimentally for each phase, and the third component was assumed to comprise the rest of the mixture.

4.3.1   Water Analysis and Confidence Intervals

Karl Fischer titration is well established as being accurate and precise, requires little sample prep, small samples and relatively short analysis times[47-48]. Furthermore Karl Fischer titration is selective to water, whereas other methods for determining water

34

content are not. The method consists of dissolving samples to be analyzed in an alcohol and performing a volumetric titration using a titrant which reacts with a known quantity of water per volume of titrant. In this work samples were dissolved in Hydranal® Methanol Dry (≤0.01% water) and titrated with Hydranal® Composite-5, a titrant that reacts with 5 mg of water per 1 mL of titrant. Titrations were performed using a Mettler-Toledo DL18 Karl Fischer Titrator.

Syringes containing samples for water analysis were weighed. Samples were injected through a septum into the titration vessel already filled with dry methanol and the empty syringe weighed. The difference in syringe mass before and after injection, corrected for buoyancy effects, was taken as the sample mass (M_{sample}). After completing a titration the instrument reported the mass of water (M_{water}) in mg titrated from the sample. The water mass was used along with the injected sample mass to calculate a mass fraction of water (MF_{water}) in the sample, shown in Equation 4.

$$MF_{water} = \frac{M_{water}}{M_{sample}} \qquad (4)$$

All water samples from both phases were analyzed in this way giving six replicates of each water concentration. The average of these six values ($\bar{x}$) is the reported water concentration. The standard deviation (s) of these six replicates was *not* assumed to be a good estimate of the population standard deviation. Reported confidence intervals (CI) were therefore calculated according to Equation 5.

35

$$CI = \bar{x} \pm \frac{ts}{\sqrt{N}} \qquad\qquad (5)$$

Here N is the number of repeated measurements (6) and t is the students-t value for a two-sided 95% confidence level with $N\text{-}1$ degrees of freedom (2.45).

4.3.2 Methyl Ester and Glycerin Analysis

An Agilent 7890 gas chromatograph (GC) with flame ionization detection (FID) was used for quantitation of glycerin and methyl esters. An automated liquid sampler (Agilent 7869B ALS) facilitated sample injections. Separation was achieved with a Supelco Equity™-1 fused silica capillary column, 30 m x 0.25 mm x 0.1 µm film thickness. All gasses were obtained from AirGas. Helium (99.995%) was used as the carrier gas, hydrogen (99.95%) as FID fuel, and Ultra-Zero Grade air as the oxidizer.

Samples from the light and heavy phases were analyzed by different methods, due to the differing compositions of the samples. Specifics of the GC methods for each phase are delineated in Table 6. Chromatograms were analyzed for peak areas and retention times which were determined using Chemstations Auto-Integrator built into the GC operating software. Calibration standards and analytical samples were each analyzed by GC five times to ensure repeatability of analytical results.

Table 6: Detailed instrument parameters for light and heavy phase methods

	Method Parameter	Light Method	Heavy Method
ALS	Pre-injection washes (A)	4 @ 6μL	4 @ 6μL
	Post-injection washes (B)	4 @ 6μL	4 @ 6μL
	Sample washes	1 @ 2μL	1 @ 2μL
	Sample injection volume	1μL	1μL
Inlet	Temperature	350°C	350°C
	Pressure	20psi	18psi
	Split ratio	100:1	100:1
	Septum purge	2mL/min	2mL/min
Column	Constant pressure	20psi	18psi
	Average velocity	36.8cm/s	30.2cm/s
	Average flow rate	1.49mL/min	1.01mL/min
	Average hold-up time	1.36min	1.65min
Oven	Initial temperature	110°C	170°C
	Hold time at initial T	1min	1min
	Ramp rate	60°C/min	15°C/min
	Final temperature	230°C	230°C
	Hold time at final T	4min	2min
	Post run temperature	320°C	320°C
	Post run hold time	4min	4min
FID	Temperature	260°C	350°C
	H2 flow rate	40mL/min	40mL/min
	Air flow rate	450mL/min	450mL/min
	Makeup He flow rate	33.3mL/min	33.3mL/min
	Data sampling frequency	50Hz	50Hz

As was previously stated, methyl caprate was added to each sample as an internal standard to assist in quantifying the sample components and reduce instrument variability. A response ratio for each analyte was calculated according to Equation 6[45-46].

$$RR = \log_{10}\left(\frac{MF_{ISTD} \times A_{analyte}}{A_{ISTD}}\right) \tag{6}$$

Here RR is the response ratio, MF_{ISTD} is the mass fraction of internal standard in the sample (analytical or calibration), A_{ISTD} is the peak area of the internal standard and $A_{analyte}$ the peak area of the analyte.

To generate calibration curves the response ratio calculated according to Equation 6 was plotted as the abscissa versus the log of the known mass fraction of analyte in the calibration standard, shown in Equation 7, for each replicate of each standard solution. Points generated in this way were fit to a line of the form $y = mx + b$ using the least squares regression package included in Microsoft Excel®.

$$Ordinate = \log_{10}\left(MF_{analyte}^{(s)}\right) \tag{7}$$

Unknown analyte concentrations in prepared analytical samples were determined by calculating the response ratio from Equation 6 for each of the five GC replicates from a given sample. The average of these five replicates was then used in conjunction with the slope (m) and intercept (b) from the calibration curve to calculate the unknown mass fraction of analyte in the analytical sample $\left(MF_{analyte}^{(a)}\right)$, shown in Equation 8.

$$MF_{analyte}^{(a)} = 10^{\left(\frac{RR-b}{m}\right)} \tag{8}$$

Because the prepared analytical sample contains the equilibrium sample diluted with methanol and internal standard, the mass fraction calculated according to

Equation 8 does not represent the mass fraction of analyte in the equilibrium sample.

Equation 9 illustrates how the mass fraction of equilibrium sample in the prepared

analytical sample ($MF^{(a)}_{equ\ sam}$ from Equation 3) was used with Equation 8 to find the

actual mass fraction of analyte in the equilibrium sample ($MF_{analyte}$).

$$MF_{analyte} = \frac{MF^{(a)}_{analyte}}{MF^{(a)}_{equ\ sam}} \tag{9}$$

4.3.3 Methyl Ester and Glycerin Confidence Intervals

The mass fraction of analyte in the six equilibrium samples extracted from each

phase was calculated according to Equation 9. The mass fraction from all six samples

was then averaged to produce the reported value. Confidence intervals were calculated

by two different methods and the reported interval corresponds to the larger of the two.

Calculated confidence intervals are reported as a percentage relative to the value in

question.

The first of these methods was propagation of measurement uncertainties.

Measured values used in mass fraction calculations included masses from an analytical

balance and peak areas from GC chromatograms. The variability in replicate GC

analyses of a single sample was very small provided the GC was working correctly.

Variations of more than about 1% in response ratios (Equation 6) from replicates of the

same sample indicated fouled operation of the GC. In such cases the source of variation

within the instrument was determined and eliminated, and new samples were analyzed. Variability in repeated measurements with the analytical balance was almost non-existent. The combined propagated error from these two sources for the mass fraction calculation of a single sample was very small compared with the sample-to-sample variation and was consequently ignored. Measurement uncertainty was therefore assumed to be equal to the standard deviation of mass fractions determined from six equilibrium samples. This standard deviation was used in the same manner previously described for the water analysis with intervals at the 95% confidence level calculated from Equation 5.

The second method was to determine a standard deviation for results obtained from a calibration curve using uncertainties in the fitted parameters m and b. This method is explained in detail by Skoog[46] and Miller[49]. The quantities S_{xx} and S_{yy} are found as follows:

$$S_{xx} = \sum_i (x_i - \bar{x})^2 \tag{10}$$

$$S_{yy} = \sum_i (y_i - \bar{y})^2 \tag{11}$$

where x_i and y_i are individual data pairs for calibration points and $\bar{x}$ and $\bar{y}$ are the average values for x and y from all calibration points. Equation 12 illustrates how S_{xx}

and S_{yy} are then used with the slope of the calibration curve (m) and the number of

calibration points on the curve N_c to find the quantity s_r.

$$s_r = \sqrt{\frac{S_{yy} - m^2 S_{xx}}{N_c - 2}} \tag{12}$$

The standard deviation for results obtained from the calibration curve (s_c) is then found

as stated in Equation 13 where y_c is the mean of a set of N replicate unknown analyses.

$$s_c = \frac{s_r}{m} \sqrt{\frac{1}{N} + \frac{1}{N_c} + \frac{(y_c - \bar{y})^2}{m^2 S_{xx}}} \tag{13}$$

The standard deviation found by means of this method was then used to

calculate a confidence interval as previously laid forth, using Equation 5. Examination

of Equation 13 indicates that s_c will be smallest when y_c is equal to $\bar{y}$ and will increase as

one deviates farther from $\bar{y}$. This was evidenced in the accepted confidence intervals.

Concentrations nearer the center of calibration curves had larger measurement

uncertainty than that calculated from this method, while very small concentrations near

the lower limit of the calibration curves tended to have larger uncertainties due to fitted

parameters than from the measurements. These errors from fitted parameters could

have been reduced by extending the lower limit of a calibration curve such that

measured concentrations were nearer the center. This discussion of calibration curve

lower limits is treated further in Section 5.2.

After experimentally determining mass fractions of the two minor components,

that of the third was calculated by difference. Mass fractions (MF_a) of all three

components were then converted to mole fractions (x_a) by assuming a basis of 1 gm and

using the molecular weight (MW_a) of each component as shown in Equation 14.

$$x_a = \frac{MF_a/MW_a}{MF_a/MW_a + MF_b/MW_b + MF_c/MW_c} \tag{14}$$

Chapter 5   Experimental Results and Discussion

5.1   Calibration Results

The calibration standards were prepared as outlined in Section 4.2.6 with mass

fractions ranging from of 1 to $1x10^{-6}$. Because the molecular weight of the compounds

varied, the mole fraction of compound in the calibration standards also varied. Because

the calibration plots that follow are in terms of calculated response ratios, the actual

mole fractions of analyte in each prepared calibration standard are shown in Tables 7

and 8.

Table 7: Mole fractions of methyl ester in prepared calibration standards

Standard	Mass Fraction	Laurate	Myristate	Palmitate	Stearate	Oleate
Pure	$1.0x10^{0}$	$1.0x10^{0}$	$1.0x10^{0}$	$1.0x10^{0}$	$1.0x10^{0}$	$1.0x10^{0}$
Dilution 1	$1.0x10^{-1}$	$1.6x10^{-2}$	$1.4x10^{-2}$	$1.3x10^{-2}$	$1.2x10^{-2}$	$1.2x10^{-2}$
Dilution 2	$1.0x10^{-2}$	$1.5x10^{-3}$	$1.3x10^{-3}$	$1.2x10^{-3}$	$1.1x10^{-3}$	$1.1x10^{-3}$
Dilution 3	$1.0x10^{-3}$	$1.5x10^{-4}$	$1.3x10^{-4}$	$1.2x10^{-4}$	$1.1x10^{-4}$	$1.1x10^{-4}$
Dilution 4	$1.0x10^{-4}$	$1.5x10^{-5}$	$1.3x10^{-5}$	$1.2x10^{-5}$	$1.1x10^{-5}$	$1.1x10^{-5}$
Dilution 5	$1.0x10^{-5}$	$1.5x10^{-6}$	$1.3x10^{-6}$	$1.2x10^{-6}$	---	---
Dilution 6	$1.0x10^{-6}$	$1.5x10^{-7}$	$1.3x10^{-7}$	$1.2x10^{-7}$	---	---

Dilutions 5 and 6 for methyl stearate and oleate calibrations were below the

reliable detection limit of the method. Dilution 6 for the glycerin calibration was also

below the detection limit. The standard prepared with pure glycerin saturated the GC

column producing poor results and was therefore omitted from the calibration.

43

Table 8: Mole fractions of glycerin in prepared calibration standards

Standard	Mass Fraction	Glycerin
Pure	1.0×10^0	---
Dilution 1	1.0×10^{-1}	3.7×10^{-2}
Dilution 2	2.0×10^{-2}	7.1×10^{-3}
Dilution 3	4.0×10^{-3}	1.4×10^{-3}
Dilution 4	8.0×10^{-4}	2.8×10^{-4}
Dilution 5	1.6×10^{-4}	5.6×10^{-5}
Dilution 6	3.2×10^{-5}	---

As explained in Section 4.3.2, calibration curves were generated by plotting Equation 6 vs. Equation 7 for each of the calibration standards and then fitting a line to the points. These plots, along with the regressed curves and correlation coefficients, are shown in Figures 3-8. Note that for each plot the standard containing the pure component appears in the upper right and that containing dilution 6 (or the lowest detectable dilution) in the lower left.
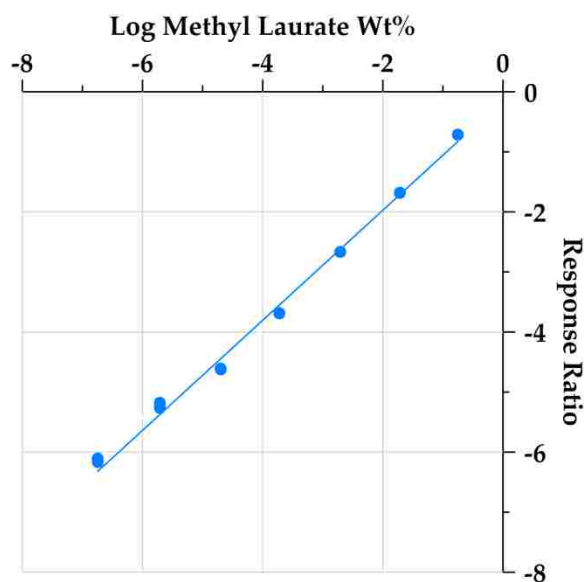
Figure 3: Methyl Laurate calibration points and fit, $R^2 = 0.994533$
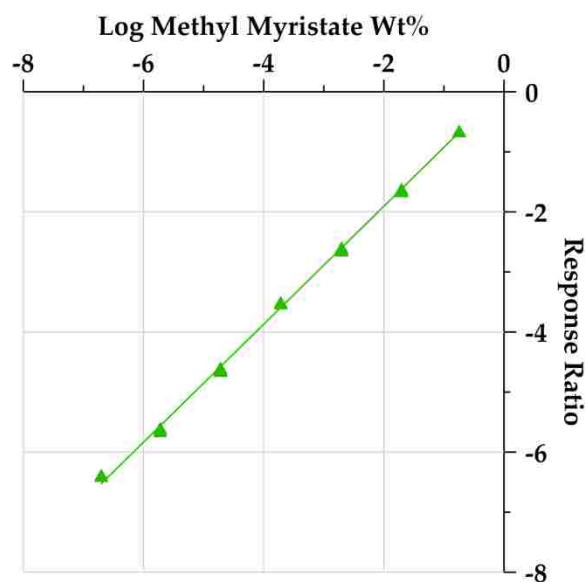
Figure 4: Methyl Myristate calibration points and fit, $R^2 = 0.998907$
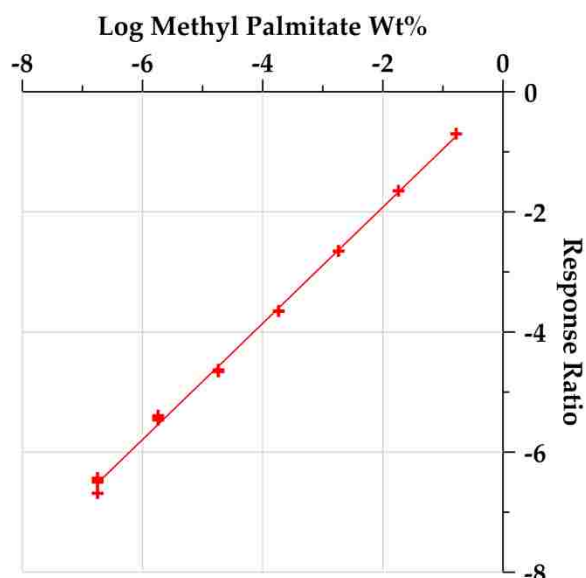
Figure 5: Methyl Palmitate calibration points and fit, $R^2 = 0.998836$
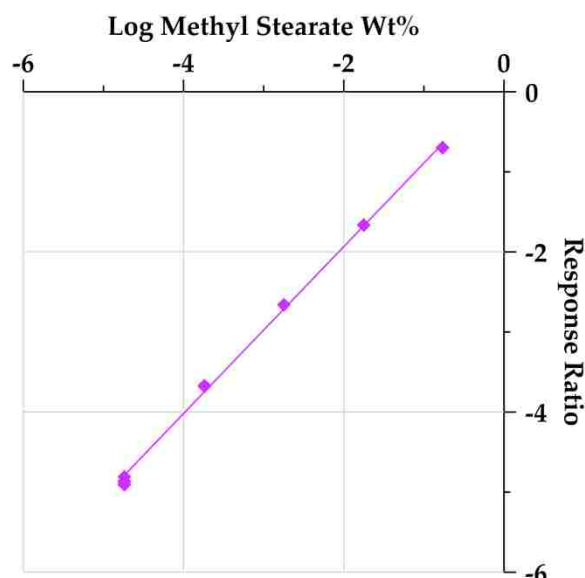
Figure 6: Methyl Stearate calibration points and fit, $R^2 = 0.998356$
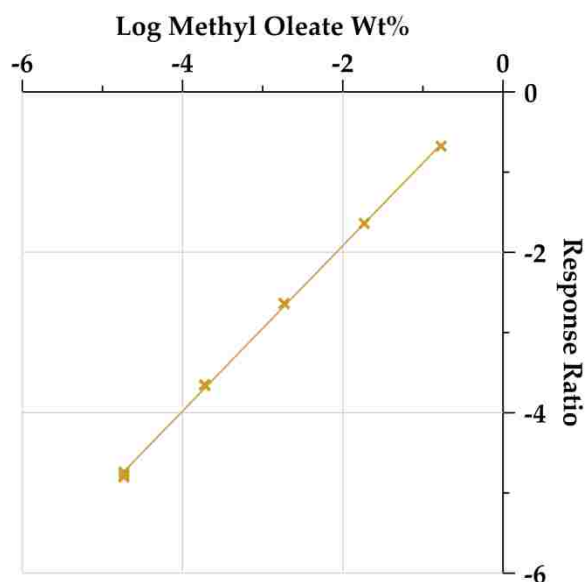
Figure 7: Methyl Oleate calibration points and fit, $R^2 = 0.999445$
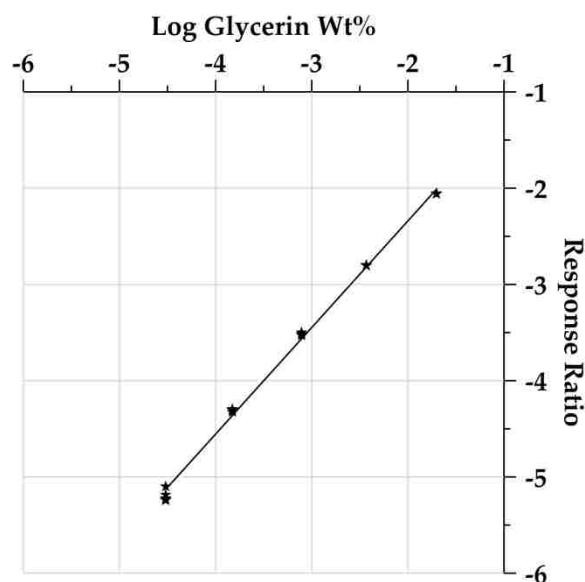
Figure 8: Glycerin calibration points and fit, $R^2 = 0.997440$

These six plots are discussed in the following section. For comparative purposes,

a single plot containing all six calibration curves and a discussion of that plot is

included in Appendix A, section A.1.

5.2   Discussion of Calibrations

As can be seen in Figures 3-8 all calibrations produced very straight lines with high correlation coefficients. With a few exceptions the repeatability between five replicate analyses of each standard was very good, as is also evidenced in the plots.

A significant amount of peak broadening was observed with the very small dilutions of the esters, producing inconsistent integration results. This resulted in some scatter, an example of which can be seen in the smallest dilution of the methyl palmitate curve, Figure 5. In the cases of methyl stearate and oleate dilutions 5 and 6 this scatter was extreme and was the justification for deeming those concentrations as below the reliable detection limit of the method. Modification of the GC method to correct the peak broadening caused the internal standard, glycerin, and solvent peaks to overlap, further complicating the issue.

A possible solution to this issue could have been to change internal standards. Methyl caprate was chosen as the standard initially because it is chemically similar to methyl laurate (two carbons shorter), and yet different enough to easily separate in the GC column. Methyl caprate was then also used as the internal standard for the remaining esters. A different approach which may have eliminated some of the aforementioned issues could have been to use the next shortest ester for each compound as an internal standard, instead of the same standard for everything. Using

methyl palmitate as the internal standard for methyl stearate and oleate analyses, as an

example, and modifying the GC method accordingly. Sharper peaks could then be

obtained with the more dilute concentrations of the heavier esters without having the

internal standard peak obscured by the solvent and glycerin peaks.

5.3 Ternary Equilibrium Results

Ternary equilibrium measurements were carried out as previously outlined in

sections 4.2 and 4.3. Errors were calculated for each point as explained in section 4.3.3

and are reported as percentages relative to the value. Experimental results are shown in

the following pages in Tables 9, 11, 13, 15 and 17. Errors included in these tables are

averaged values for each component in each phase, unless otherwise noted. Extended

tables showing the individual errors for each point are included in section A.2.

Data sets were fitted with the Non-Random Two-Liquid (NRTL) activity

coefficient model[50-51]. Fitting was accomplished using the data fitting package included

in Aspen Plus ®. The maximum likelihood objective function (Q) was minimized by the

data regression and is shown in Equation 15 with P equal to the number of phases (2), T

the number of tie lines (which varied with the system), and C the number of

components (3).

$$Q = \sum_i^P \sum_j^T \sum_k^{C-1} \left(\frac{x_{i,j,k}^{calc} - x_{i,j,k}^{exp}}{\sigma_{x,i,j,k}^{exp}} \right)^2 \qquad \textbf{(15)}$$

Experimental values are represented by x^{exp} and the calculated or predicted values by x^{calc}. This objective function also makes use of the experimental errors for each point (σ^{exp}) as calculated in Section 4.3.

Equation 16 shows how activity coefficients γ_i were found from the NRTL model. Values for G_{ij} were found using Equation 17 with $\alpha_{ji} = \alpha_{ij} = 0.2$ as is commonly used for systems which exhibit liquid immiscibility. Values for the dimensionless parameter τ_{ij} were fitted directly and are reported in Tables 10, 12, 14, 16 and 18.

$$\ln \gamma_i = \frac{\sum_j x_j \tau_{ji} G_{ji}}{\sum_k x_k G_{ki}} + \sum_j \frac{x_j G_{ij}}{\sum_k x_k G_{kj}} \left(\tau_{ij} - \frac{\sum_m x_m \tau_{mj} G_{mj}}{\sum_k x_k G_{kj}} \right) \tag{16}$$

$$G_{ij} = exp(-\alpha_{ij}\tau_{ij}) \tag{17}$$

Ternary diagrams are not clearly illustrative for systems with very low mutual solubility. They appear as essentially pure component on one end of the tie lines and a binary mixture on the other. However, they do show agreement of initial charges with measured tie-line data and agreement of tie-lines generated from an NRTL fit with experimental tie-lines. They are included here in Figures 9, 12, 15, 18 and 21. The NRTL tie-lines are not intended to lie directly on top of experimental tie-lines, merely to indicate that the slopes are similar and follow the same pattern through the two phase region.

5.3.1 Methyl Laurate Tables and Figures

Table 9: Mole fraction tie-line data: Methyl Laurate (x_1) – Water (x_2) – Glycerin (x_3)

Ester Phase			Water/Glycerin Phase		
x_1 (calc)	$x_2 \pm 3\%$	$x_3 \pm 11\%$	$x_1 \pm 31\%$	$x_2 \pm 1\%$	x_3 (calc)
0.9958	0.0003[a]	0.0039	2.4×10^{-5}	0.0025[d]	0.9974
0.9918	0.0045	0.0037	2.1×10^{-5}	0.1166	0.8833
0.9891	0.0077	0.0032	1.5×10^{-5}	0.2168	0.7832
0.9850	0.0122	0.0029	1.1×10^{-5}	0.3162	0.6838
0.9774	0.0204	0.0023	7.0×10^{-6}	0.5052	0.4948
0.9667	0.0320	0.0013	2.6×10^{-6}	0.7253	0.2747
0.9573	0.0423	0.0004[b]	2.1×10^{-7}	0.8892	0.1108
0.9515	0.0485	0.0000	2.5×10^{-7}	1.0000	0.0000[e]

a ± 25%, *b* ± 52%, *d* ± 10%, *e* Verified by GC

Table 10: NRTL parameters:
Methyl Laurate (x_1) – Water (x_2) – Glycerin (x_3)

i	j	τ_{ij}	τ_{ji}
1	2	2.49	13.45
1	3	4.15	8.89
2	3	1.33	-1.09
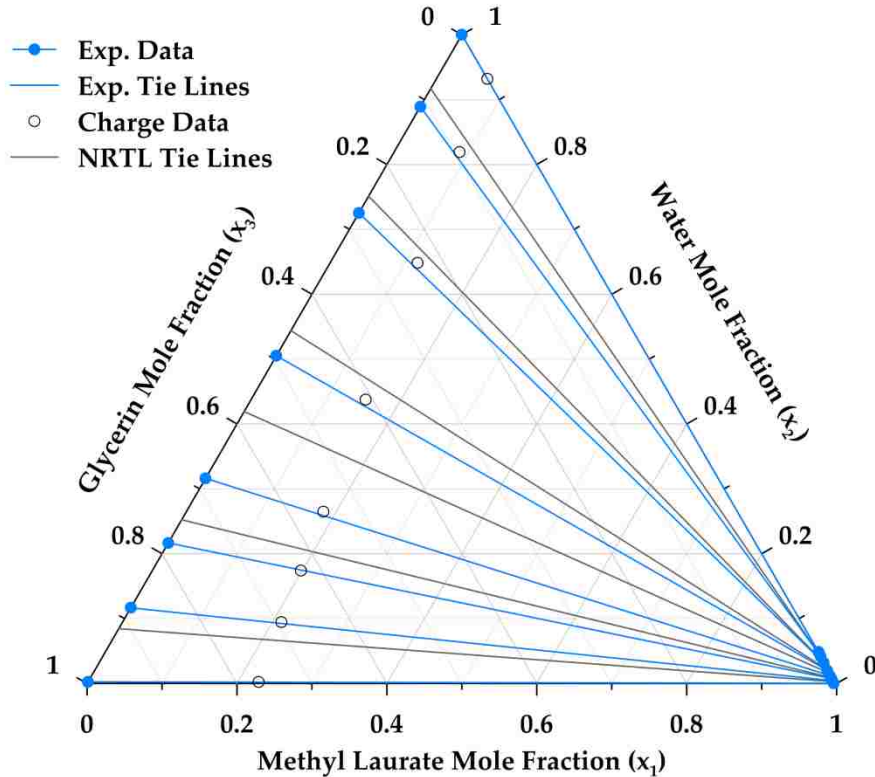
Figure 9: Ternary diagram: Methyl Laurate (x_1) – Water (x_2) – Glycerin (x_3)

Figure 10: Light phase close up: Methyl Laurate (x_1) – Water (x_2) – Glycerin (x_3) showing individual error bars and NRTL fit

Figure 11: Heavy phase close up: Methyl Laurate (x_1) – Water (x_2) – Glycerin (x_3) showing individual error bars and NRTL fit

5.3.2 Methyl Myristate Tables and Figures

Table 11: Mole fraction tie-line data: Methyl Myristate (x_1) – Water (x_2) – Glycerin (x_3)

Ester Phase			Water/Glycerin Phase		
x_1 (calc)	$x_2 \pm 4\%$	$x_3 \pm 13\%$	$x_1 \pm 50\%$	$x_2 \pm 1\%$	x_3 (calc)
0.9960	0.0011[a]	0.0029	8.3×10^{-6}	0.0024[d]	0.9976
0.9935	0.0041	0.0025	6.8×10^{-6}	0.1163	0.8837
0.9904	0.0072	0.0024	4.7×10^{-6}	0.2099	0.7901
0.9869	0.0110	0.0021	3.3×10^{-6}	0.3166	0.6834
0.9799	0.0184	0.0017	9.6×10^{-7}	0.5055	0.4945
0.9706	0.0286	0.0008	2.9×10^{-7}	0.7232	0.2768
0.9635	0.0363	0.0002[b]	$< 1 \times 10^{-7}$	0.8883	0.1117
0.9579	0.0421	0.0000	$< 1 \times 10^{-7}$	1.0000	0.0000[e]

a ± 28%, *b* ± 87%, *d* ± 10%, *e* Verified by GC

Table 12: NRTL parameters:
Methyl Myristate (x_1) – Water (x_2) – Glycerin (x_3)

i	j	τ_{ij}	τ_{ji}
1	2	2.79	15.01
1	3	4.66	9.95
2	3	0.93	-0.77
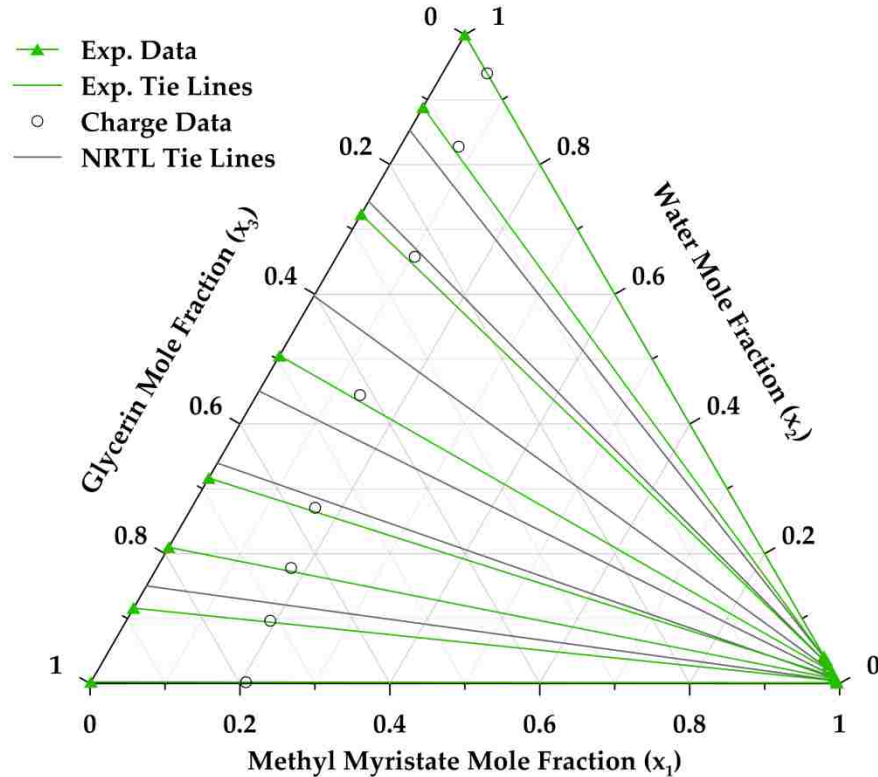
Figure 12: Ternary diagram: Methyl Myristate (x_1) – Water (x_2) – Glycerin (x_3)
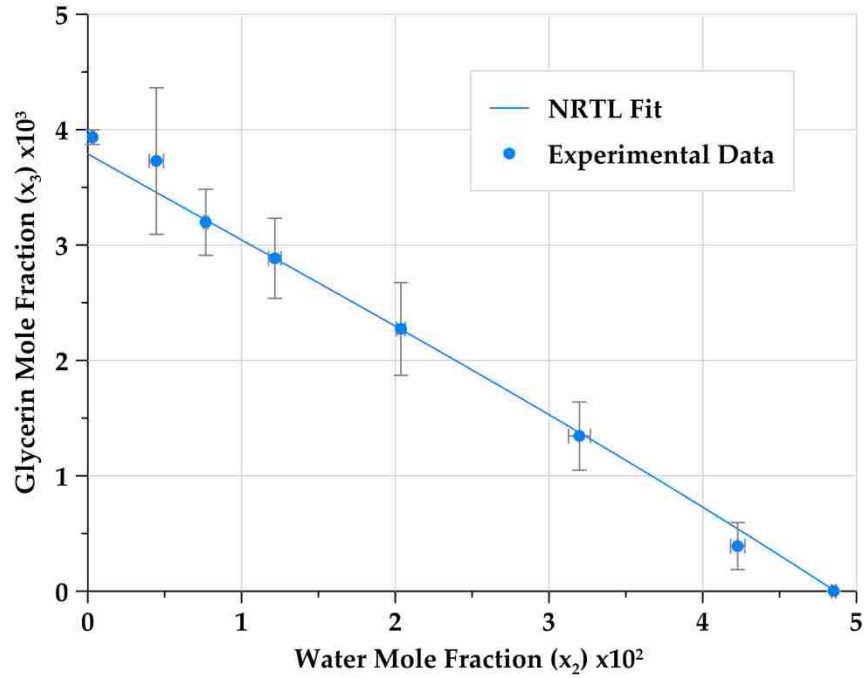
Figure 13: Light phase close up: Methyl Myristate (x_1) – Water (x_2) – Glycerin (x_3) showing individual error bars and NRTL fit

Figure 14: Heavy phase close up: Methyl Myristate (x_1) – Water (x_2) – Glycerin (x_3) showing individual error bars and NRTL fit

5.3.3 Methyl Palmitate Tables and Figures

Table 13: Mole fraction tie-line data: Methyl Palmitate (x_1) – Water (x_2) – Glycerin (x_3)

Ester Phase			Water/Glycerin Phase		
x_1 (calc)	$x_2 \pm 6\%$	$x_3 \pm 18\%$	$x_1 \pm 50\%$	$x_2 \pm 3\%$	x_3 (calc)
0.9960	0.0010[a]	0.0031	8.5×10^{-6}	0.0033[d]	0.9967
0.9933	0.0038	0.0029	4.5×10^{-6}	0.1141	0.8859
0.9906	0.0066	0.0028	1.7×10^{-6}	0.2088	0.7912
0.9873	0.0103	0.0025[b]	1.4×10^{-6}	0.3133	0.6867
0.9803	0.0179	0.0018	8.4×10^{-7}	0.5066	0.4934
0.9697	0.0293	0.0010[b]	$< 1 \times 10^{-7}$	0.7869	0.2131
0.9608	0.0392	0.0000	$< 1 \times 10^{-7}$	0.9531	0.0469

a ± 39%, b ± 57%, d ± 10%

Table 14: NRTL parameters:
Methyl Palmitate (x_1) – Water (x_2) – Glycerin (x_3)

i	j	τ_{ij}	τ_{ji}
1	2	2.97	16.49
1	3	4.64	10.48
2	3	1.33	-1.09
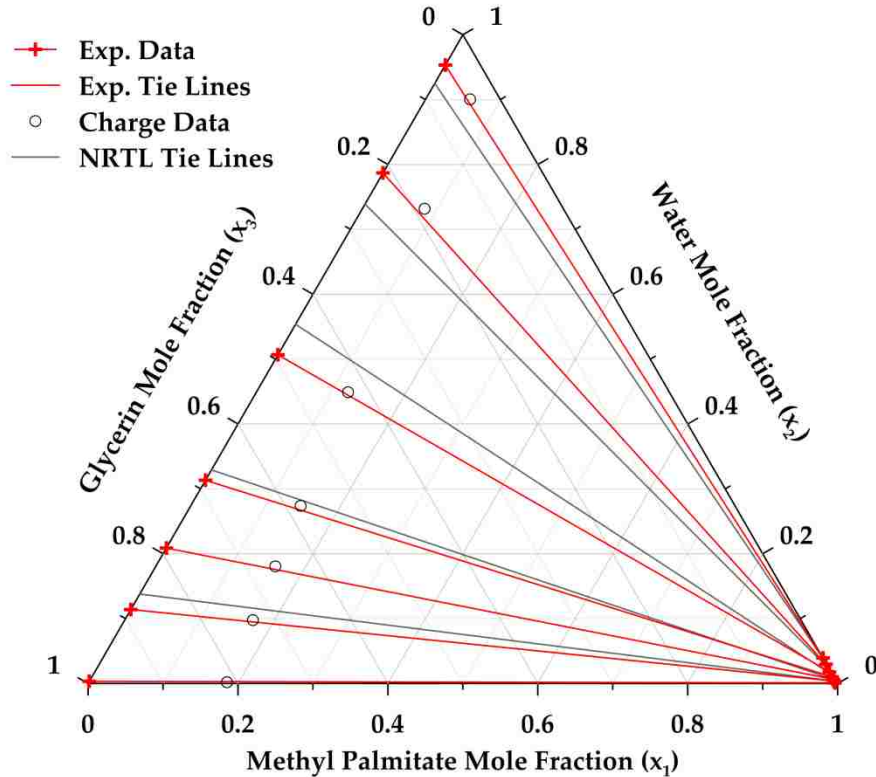
Figure 15: Ternary diagram: Methyl Palmitate (x_1) – Water (x_2) – Glycerin (x_3)

Figure 16: Light phase close up: Methyl Palmitate (x_1) – Water (x_2) – Glycerin (x_3) showing individual error bars and NRTL fit
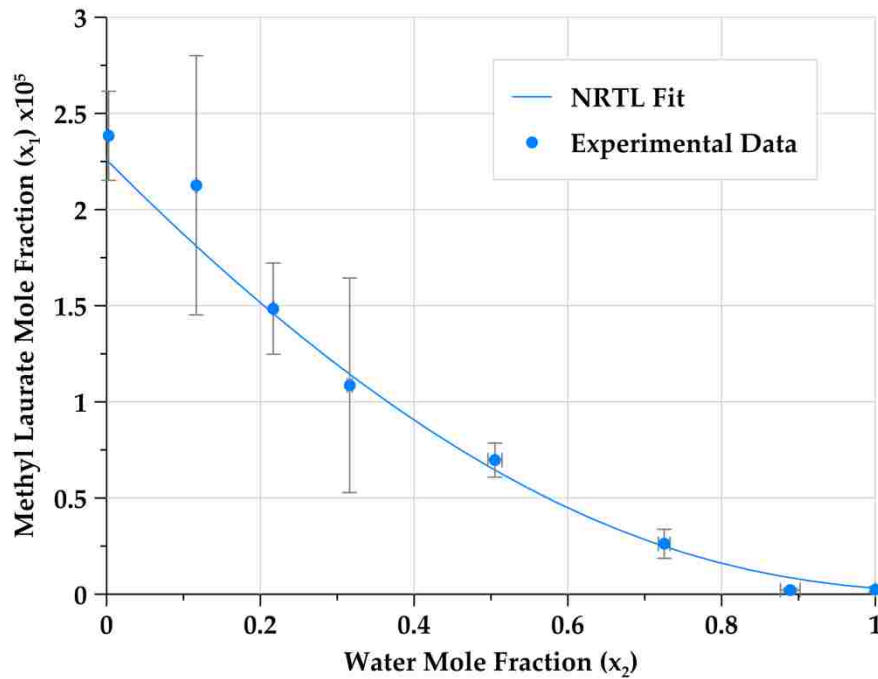

Figure 17: Heavy phase close up: Methyl Palmitate (x_1) – Water (x_2) – Glycerin (x_3) showing individual error bars and NRTL fit

5.3.4 Methyl Stearate Tables and Figures

Table 15: Mole fraction tie-line data: Methyl Stearate (x_1) – Water (x_2) – Glycerin (x_3)

Ester Phase			Water/Glycerin Phase		
x1 (calc)	x2 ± 7%	x3 ± 33%	x1 ± 49%	x2 ± 1%	x3 (calc)
0.9913	0.0029*a*	0.0058	2.6x10-6	0.0809	0.9191
0.9890	0.0062	0.0048*b*	1.9x10-6	0.2084	0.7916
0.9843	0.0096	0.0060	1.3x10-6	0.3141	0.6859
0.9802	0.0168	0.0031	< 1x10-6	0.5021	0.4979

a ± 36%, *b* ± 77%

Table 16: NRTL parameters:
Methyl Stearate (x_1) – Water (x_2) – Glycerin (x_3)

| i	j	τ_{ij}	τ_{ji}
1	2	3.11	16.42
1	3	3.96	10.96
2	3	0.61	-0.37

Figure 18: Ternary diagram: Methyl Stearate (x_1) – Water (x_2) – Glycerin (x_3)
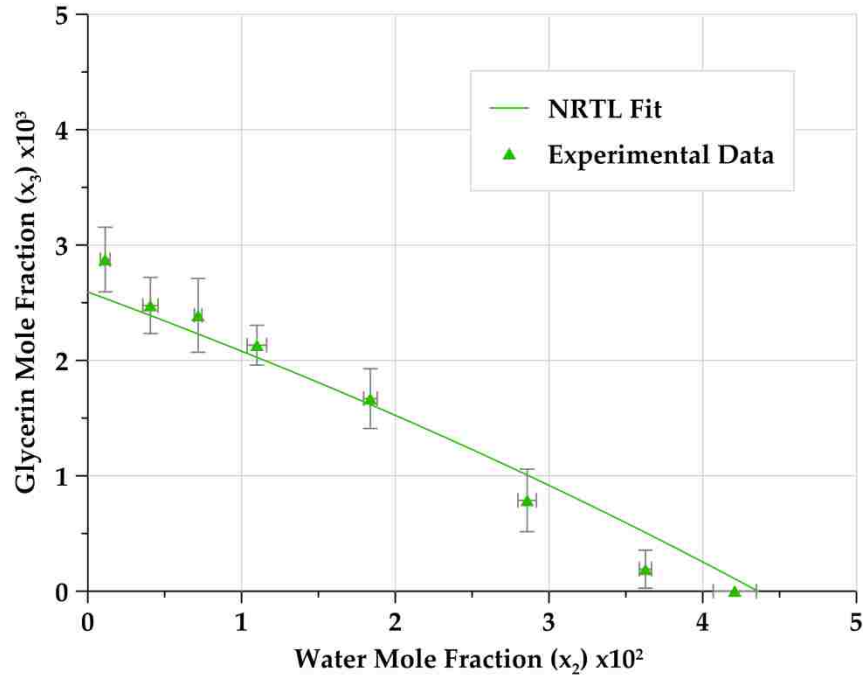
Figure 19: Light phase close up: Methyl Stearate (x_1) – Water (x_2) – Glycerin (x_3) showing individual error bars and NRTL fit
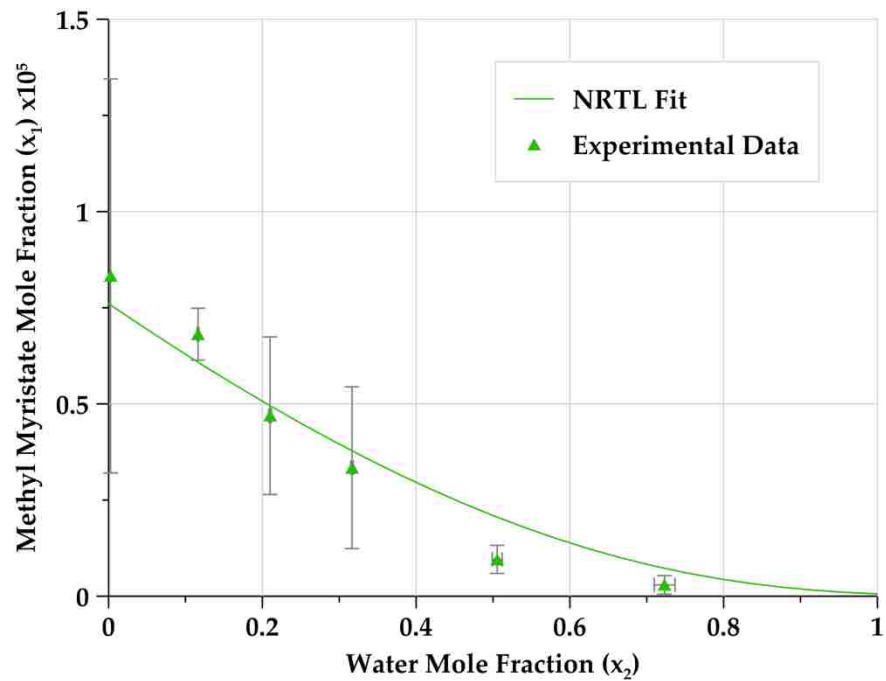

Figure 20: Heavy phase close up: Methyl Stearate (x_1) – Water (x_2) – Glycerin (x_3) showing individual error bars and NRTL fit

5.3.5 Methyl Oleate Tables and Figures

Table 17: Mole fraction tie-line data: Methyl Oleate (x_1) – Water (x_2) – Glycerin (x_3)

Ester Phase			Water/Glycerin Phase		
x_1 (calc)	$x_2 \pm 6\%$	$x_3 \pm 16\%$	$x_1 \pm 63\%$	$x_2 \pm 2\%$	x_3 (calc)
0.9953	0.0006[a]	0.0042	9.2×10^{-6}	0.0028[d]	0.9972
0.9930	0.0036	0.0034	6.1×10^{-6} [c]	0.0825	0.9175
0.9893	0.0077	0.0030	6.3×10^{-6}	0.2169	0.7831
0.9862	0.0110	0.0028	$< 1 \times 10^{-6}$	0.3166	0.6834
0.9814	0.0166	0.0020	$< 1 \times 10^{-6}$	0.5090	0.4910
0.9692	0.0295	0.0013	$< 1 \times 10^{-6}$	0.7276	0.2724
0.9618	0.0376	0.0005[b]	$< 1 \times 10^{-6}$	0.8954	0.1046
0.9574	0.0426	0.0000	$< 1 \times 10^{-6}$	1.0000	0.0000[e]

a ± 44%, *b* ± 59%, *c* ± 177%, *d* ± 10%, *e* Verified by GC

Table 18: NRTL parameters:
Methyl Oleate (x_1) – Water (x_2) – Glycerin (x_3)

| i	j	τ_{ij}	τ_{ji}
1	2	2.68	14.25
1	3	4.33	9.79
2	3	1.33	-1.09
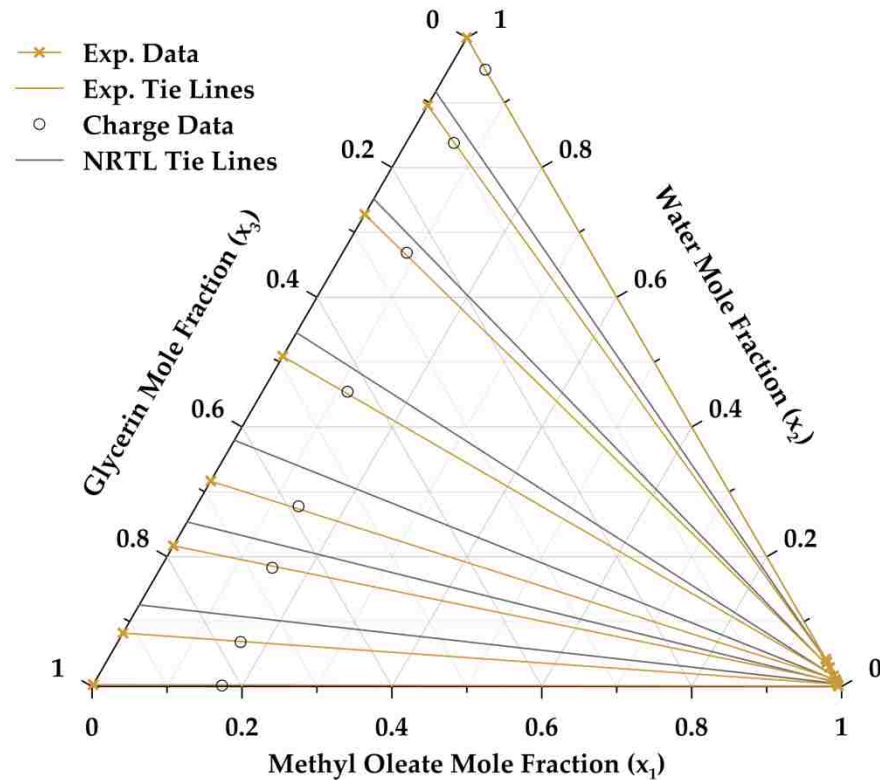
Figure 21: Ternary diagram: Methyl Oleate (x_1) – Water (x_2) – Glycerin (x_3)
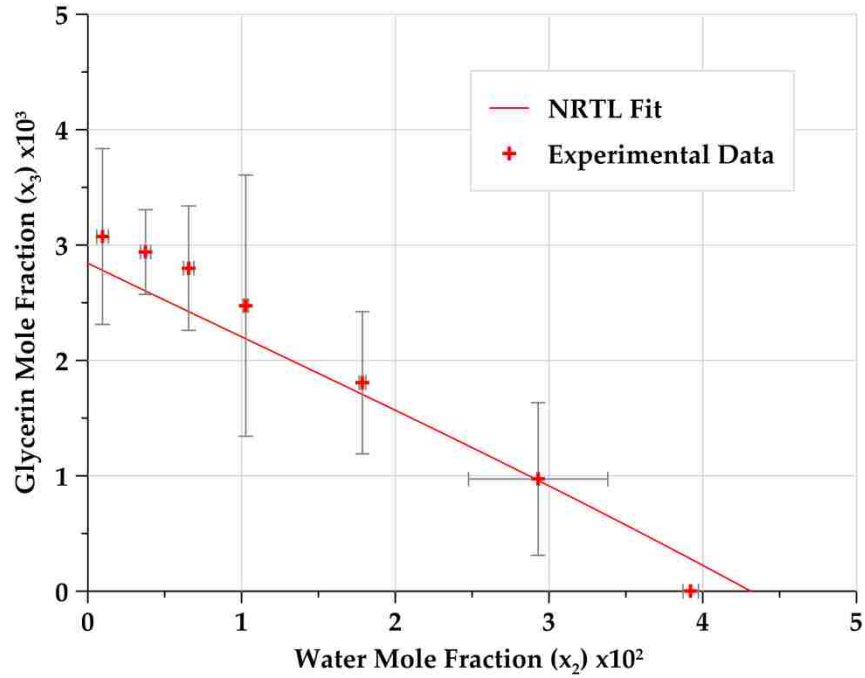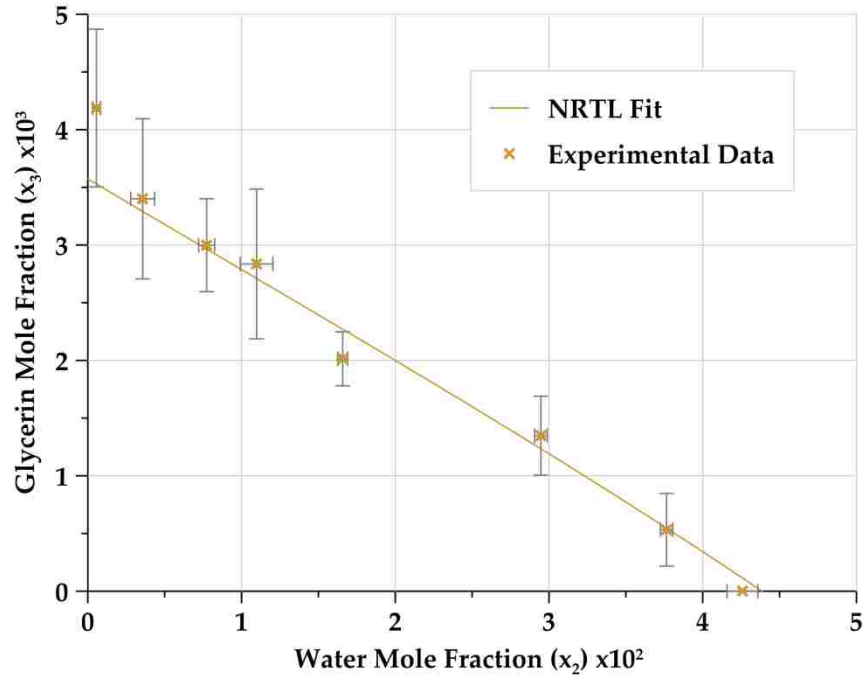
Figure 22: Light phase close up: Methyl Oleate (x_1) – Water (x_2) – Glycerin (x_3) showing individual error bars and NRTL fit
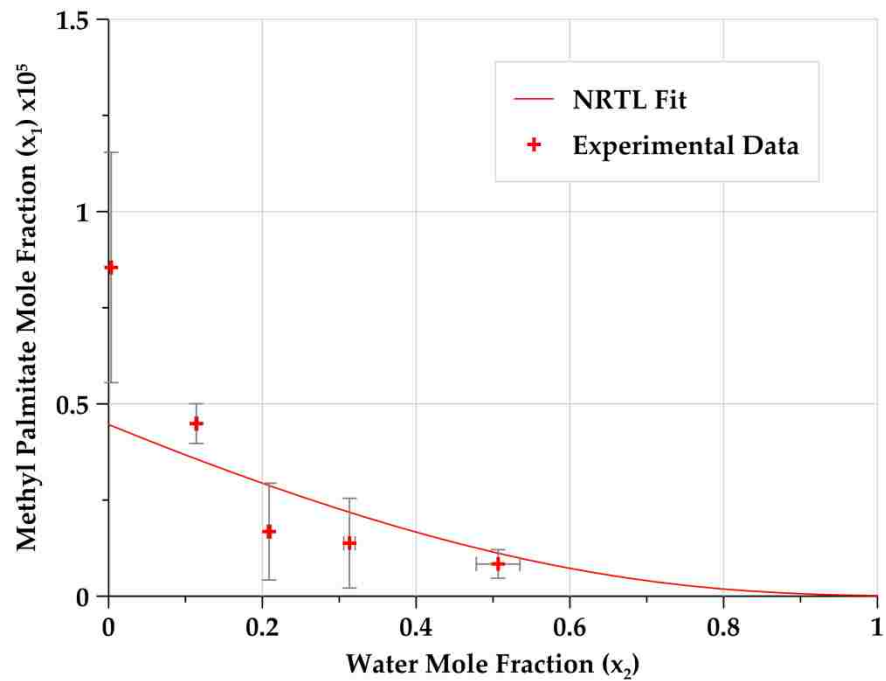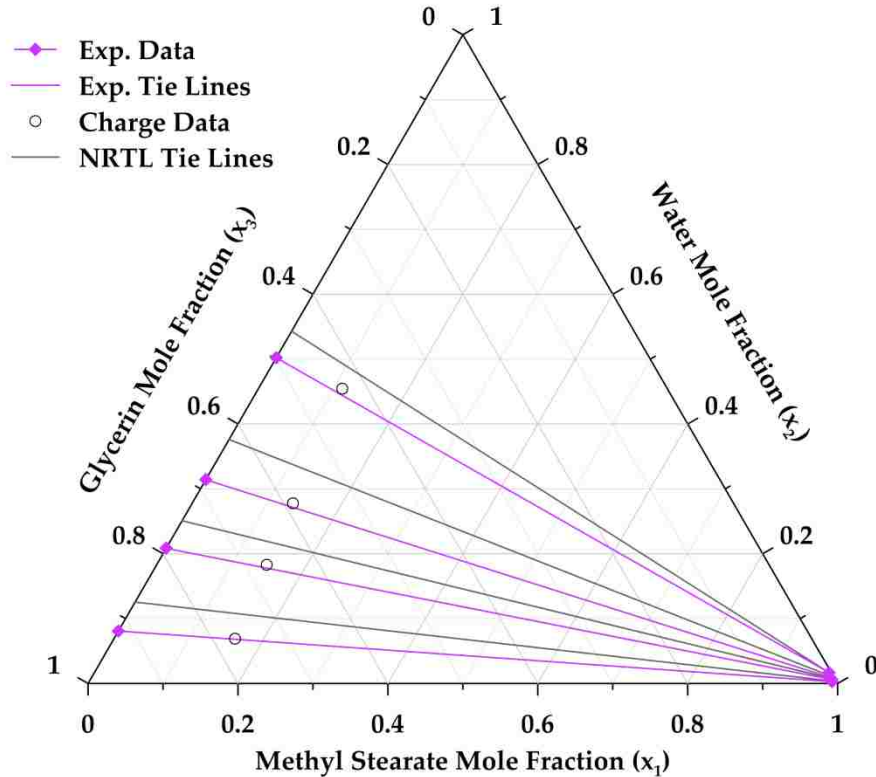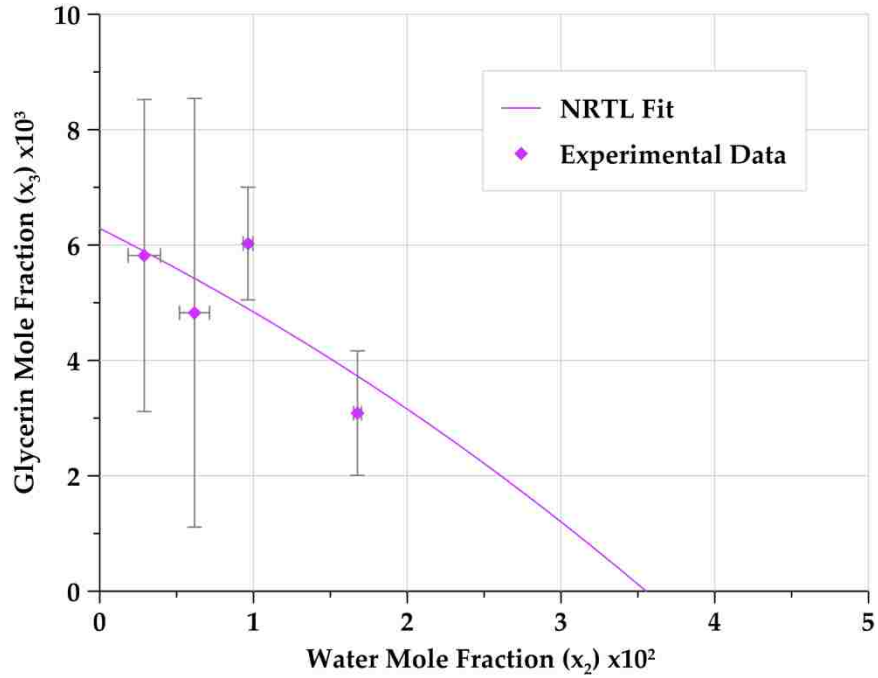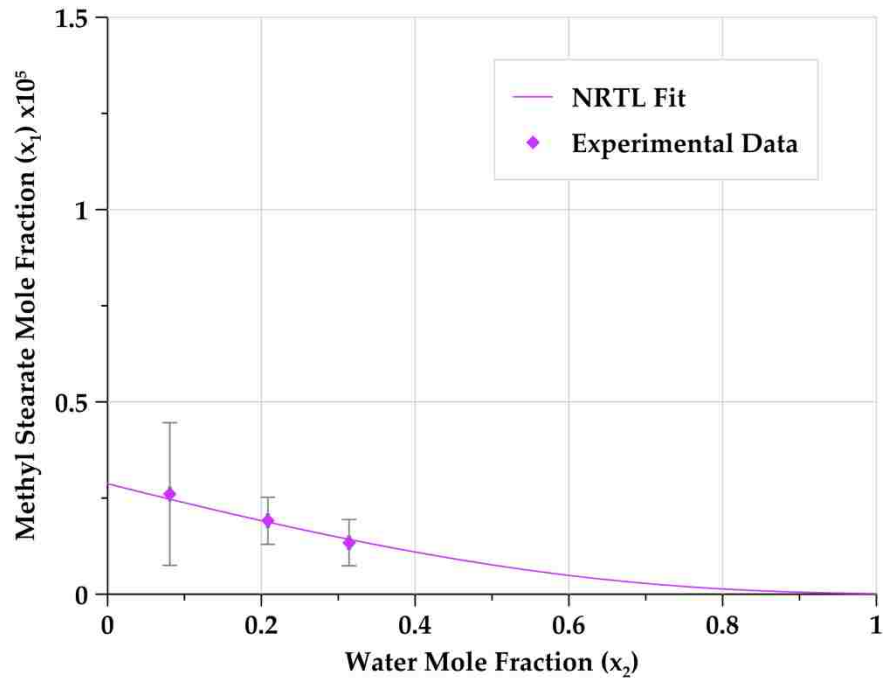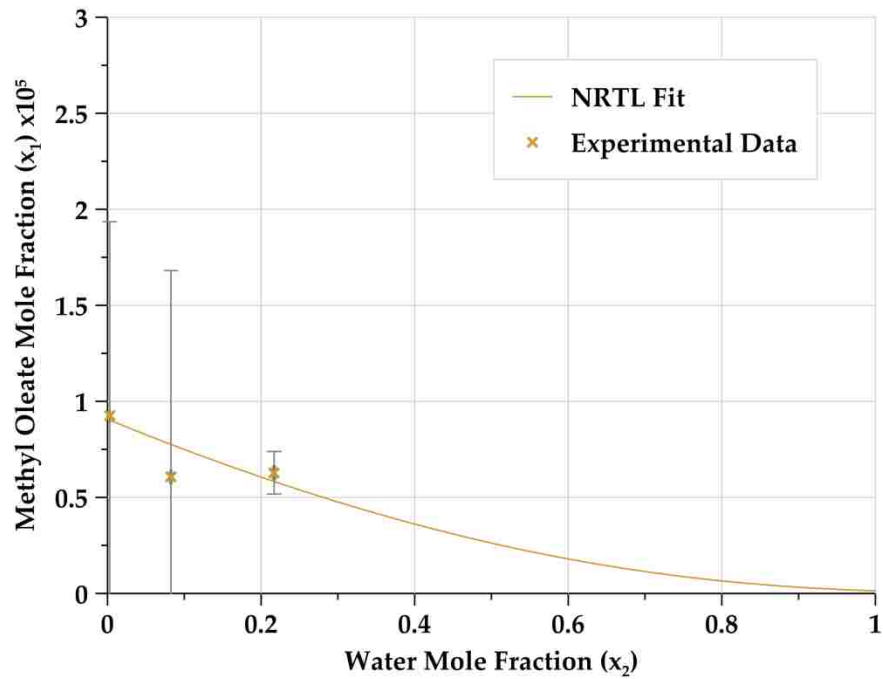

Figure 23: Heavy phase close up: Methyl Oleate (x_1) – Water (x_2) – Glycerin (x_3) showing individual error bars and NRTL fit

In addition to ternary diagrams, a plot of each end of the tie-lines is also included

showing only concentrations of components which were experimentally determined.

Plots of the light phase glycerin vs. water mole fractions with individual two

dimensional error bars and the NRTL fit are shown in Figures 10, 13, 16, 19 and 22.

Similar plots of heavy phase methyl ester vs. water mole fractions are also shown in

Figures 11, 14, 17, 20 and 23. These plots were constructed such that reading from left

to right the first point encountered on each pair of plots corresponds to opposite ends of

the same tie-line.

5.4 Discussion of Ternary Results

In general the results for each individual system appear to be relatively self-

consistent. While the NRTL fits are not perfect, they follow the appropriate trends and

roughly follow the shape of the data. Comparisons between the different systems are

made for each phase in the following sections.

The obvious exception to the previous statement is the methyl stearate system

(Section 5.3.4), which shows large scatter and extreme errors in the light phase

compared with all other systems. Significant difficulties were encountered measuring

this system due to the relatively high melting point of methyl stearate (39 °C).

Experimental methods required sample preparation and analysis to occur with the

sample at room temperature, yet the melting point of methyl stearate is well above that.

Extracted samples froze quickly in syringes, needles, and sample tubing making the accurate transfer of samples difficult.

Analysis was further complicated by the low solubility of methyl stearate in methanol at room temperature. Prepared analytical samples and the ALS had to be maintained at approximately 40 °C to keep methyl stearate in solution. Even with these precautions there was significant buildup of solid methyl stearate in the ALS syringe, as well as in the GC injection port and on the FID jet. Because of these complications and the highly inconsistent results produced, measurements with methyl stearate were terminated before the system was completed. The experimental results obtained and NRTL fit of the methyl stearate data are included in Section 5.3.4 and in the following discussion for thoroughness; however, it is not suggested that they are an accurate representation of the system's behavior.

Another point deserving some discussion is the NRTL fit of the heavy phase methyl palmitate data shown in Figure 17. The data are poorly correlated with the NRTL fit shown. The NRTL equation is not capable of fitting such sharp curvature in the extremely small concentration range represented by these data. Additionally, in selecting the optimal NRTL fits included here trends across the family of systems were taken into consideration. This methyl palmitate fit was selected because it fit the family

trend even though it isn't the best fit of the data. A discussion and plot of the family

trend are included in Section 5.4.2.

A noteworthy observation regarding the ternary diagrams is that in many cases

the charge compositions do not lie directly on experimental tie lines as they should.

The charge compositions are somewhat high in water content compared to where the

tie line passes. This discrepancy increases as the overall water content of the mixture

increases.

As was discussed in Section 4.2.3, the charged cell was purged by a vacuum and

pressure cycle prior to equilibration. During the vacuum purge water in the cell could

be observed gently bubbling, and ice water cooled traps in the vacuum line showed

some condensation. Based on these observations and the high vapor pressure of water

compared with the other components present, it is likely that some water escaped from

the cell during purging. This would cause the actual mixture composition that was

allowed to equilibrate to have a lower water concentration than the charge

measurements would otherwise suggest. This shift in the charge composition could

account for the charge points having more water than the tie lines would otherwise

suggest.

The amount of water that would account for this difference was computed

based on the intersection of a tie-line with a line passing through the water apex (a

water mole fraction of 1) and the corresponding charge point. These calculations

indicate that in the worst cases the difference between tie-lines and charge points

corresponds to a decrease of 1% or less in the overall water composition of the system.

This corresponds to approximately 200mg of lost water in the worst cases. It seems

reasonable that over the course of three vacuum cycles each lasting several minutes

200mg of water could have been removed. In retrospect a cold trap installed in the

vacuum line and weighed before and after purging could have been used to capture

and quantify this lost water.

5.4.1 Light Phase Comparisons

Results for the light phase measurements were similar to prior expectations.

There is an inverse relationship between water and glycerin concentrations in the ester

phase. This relationship is noticeably more linear than was originally expected. In fact

a simple linear regression fits the light phase results very well giving R^2 values of at

least 0.99 for three of the four completed systems and 0.97 for the fourth.

A comparison of the light phase results for all systems is shown in Figure 24.

Initial inspection shows the systems are very similar. There is a possible trend (omitting

the methyl stearate results) although the differences from one system to the next are

small. As the carbon chain attached to a methyl ester group gets longer, one might

expect the ester to exhibit more hydrocarbon character and show less affinity for water

and glycerin. This trend is somewhat visible in Figure 24. The largest amount of water

and glycerin is seen in methyl laurate. The amount of water and glycerin found in

methyl myristate and methyl palmitate, while very similar between the two, is

somewhat less than that found in methyl laurate. Methyl oleate appears roughly

between the laurate and myristate/palmitate groups. Methyl oleate has a double bond

in the middle of the carbon chain, which could account for a small increase in its affinity

for glycerin and water. Taking into consideration the experimental error, these results

are all highly similar.
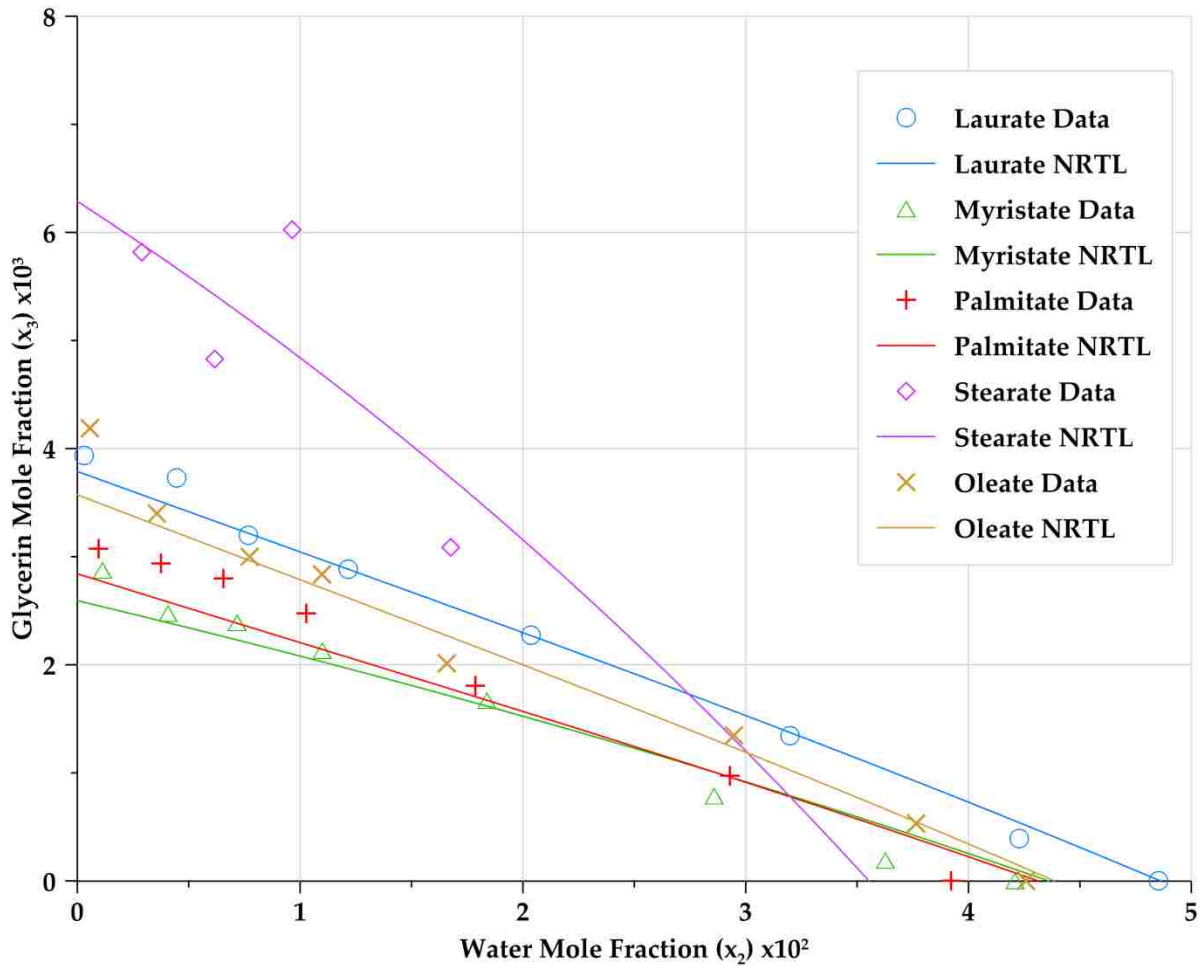
Figure 24: Comparison of light phase results for all five systems

5.4.2 Heavy Phase Comparisons

Heavy phase results show an inverse relationship between water and ester concentrations in the glycerin phase, as was expected. This trend is not as linear as the similar trend in the light phase. A comparison of the heavy phase results for all systems is shown in Figure 25.
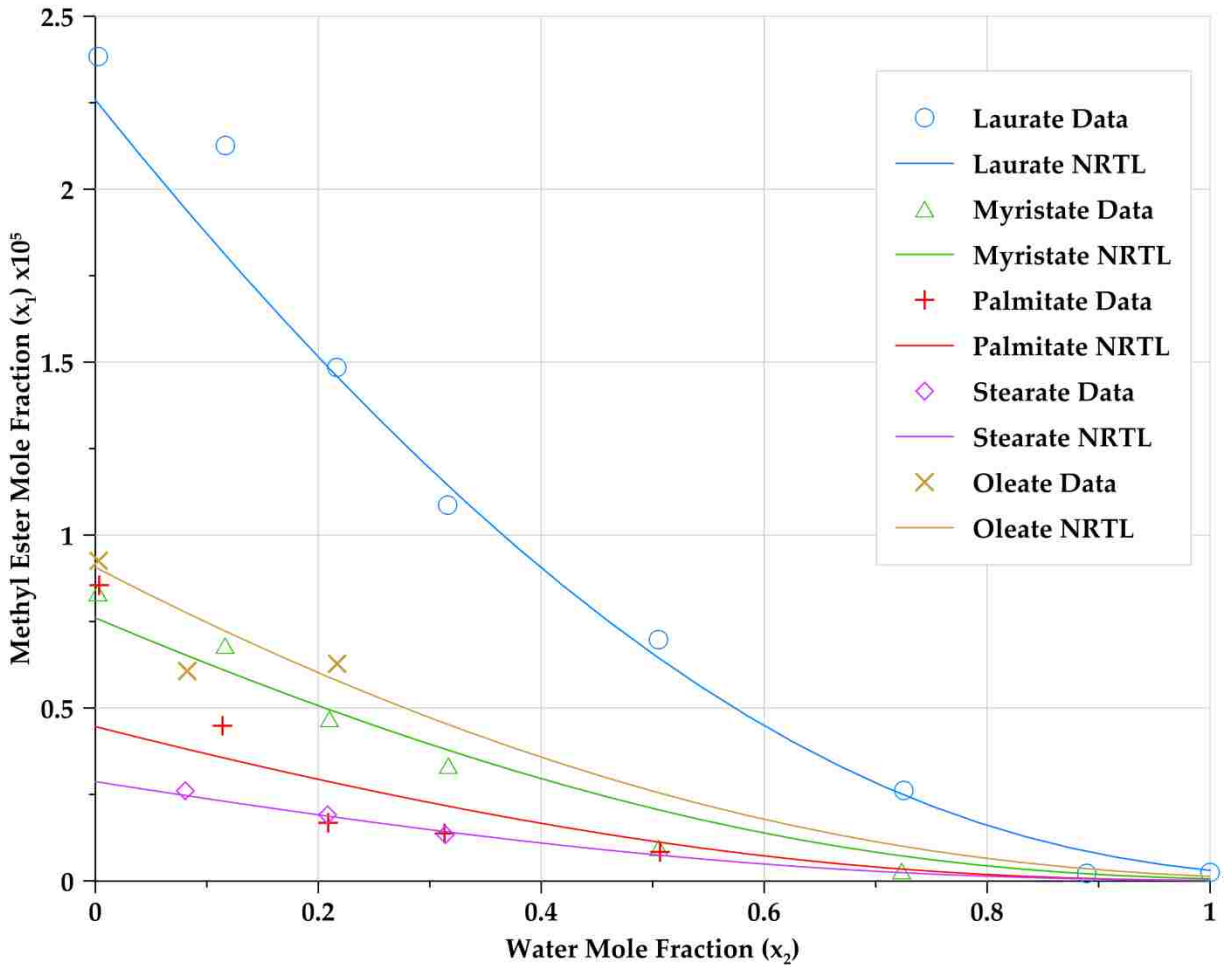
Figure 25: Comparison of heavy phase results for all five systems

A similar sort of trend related to the carbon chain length like unto that discussed for the light phase can also be observed in the heavy phase results. The longer carbon

chains show less affinity for the water and glycerin and therefore have smaller

concentrations of ester in the water/glycerin phase. Again oleate appears higher than its

carbon chain length would dictate, explainable by the presence of a double bond. A

noticeable distinction between this trend in the heavy phase and its counterpart in the

light phase is that in the heavy-phase methyl laurate is far removed from the remainder

of the systems.

A significant difference between the two phases which should be noted is the

order of magnitude of concentrations. The fraction of ester in the water/glycerin phase

is much smaller than the fractions of water and glycerin in the ester phase. The very

small concentrations of ester in the heavy phase became increasingly difficult to

measure with the larger esters. This issue and a potential solution which was not

explored were previously discussed in Section 5.2. The difficulty measuring small

concentrations of the heavier compounds is the reason that several of the data sets

shown in Figure 25 (and the tables in Section 5.3 from which they came) have fewer

points than their light-phase counterparts.

Chapter 6   Conclusions and Recommendations

An experimental apparatus and method were developed for measurement of ternary liquid-liquid equilibrium. Using this apparatus and method, ternary tie-line data were measured for five systems consisting of a methyl ester, glycerin, and water. These data fill an important gap in the literature regarding mixture properties of biodiesel and associated by-products. The data were fitted with the NRTL activity coefficient model.

The results of these experiments show extraction with water to be a promising technology for biodiesel production. Water exhibits many of the characteristics of a desirable solvent for liquid extraction of glycerin and methyl esters[52]. Some of these desirable properties include a high selectivity for the glycerin by-product relative to the methyl ester product, very minimal solubility in the methyl ester product, and lower viscosity than glycerin to promote phase separation. Additionally water is inexpensive, safe, and environmentally friendly. A potential drawback of using water for this extraction is the formation of emulsions. Experiments showed excessive time may be required for the phases to fully disengage in the event of a finely dispersed emulsion.

The separation attainable between the methyl ester product and glycerin by-product by extraction with water is as good as or better than other solvents which have been investigated[31, 53]. Other investigators have suggested that the separation requires 4 theoretical stages[30]. The Hunter-Nash equilibrium stage method[52] using the results presented here for methyl oleate suggests that 3 theoretical stages may suffice. However, further purification of the methyl ester product will still be required. ASTM standards require a methyl ester content of 99.65%[20] for biodiesel products. While some of the systems measured approach this value, none of them reaches it indicating the necessity of further purification.

The data and activity coefficient parameters presented in this work can be useful in optimizing biodiesel processes. Improved efficiency from optimized processes can enable biodiesel to gain more widespread use as an economical renewable transportation fuel.

6.1 Recommendations for Future Work

There are several continuations of the work presented here that should be explored. The first is use of an alternate internal standardization method to improve resolution towards the lower end of the concentration curves. This has already been discussed in Sections 5.2 and 5.4.2. This could potentially decrease the experimental error and provide some clarification of the trends observed across the series of esters.

As outlined in Section 2.3.1, ethanol has been investigated for biodiesel production in addition to methanol. It is an attractive alcohol for biodiesel production because it can be derived from natural sources as was discussed in Section 2.2. Using ethanol derived from biological fermentation enables biodiesel production from entirely renewable feedstocks. A valuable continuation of this work would be to measure ternary systems of the ethyl esters with water and glycerin. A group of the most commonly occurring ethyl esters were originally included in the scope of this work as indicated in Table 4; however, they were omitted due to time constraints.

A final recommendation for continuation of the work presented here is to explore the temperature dependence of these ternary systems. At various times throughout experimentation, equilibrated phases were cooled in one way or another. It was immediately apparent that equilibrium compositions were fairly temperature dependent. Upon cooling only a few degrees the phases clouded, indicating a shift in the equilibrium position. This temperature dependence was only observed, never explored or measured. Understanding how the equilibrium compositions depend on temperature would be useful in designing and optimizing separation systems and could lead to an extraction that does not require further downstream purification of the biodiesel product.

Appendix A - Supplemental Tables and Figures

A.1   Calibrations

As a continuation of the discussion in Section 5.1, a single plot showing the results of all six calibrations is shown here.
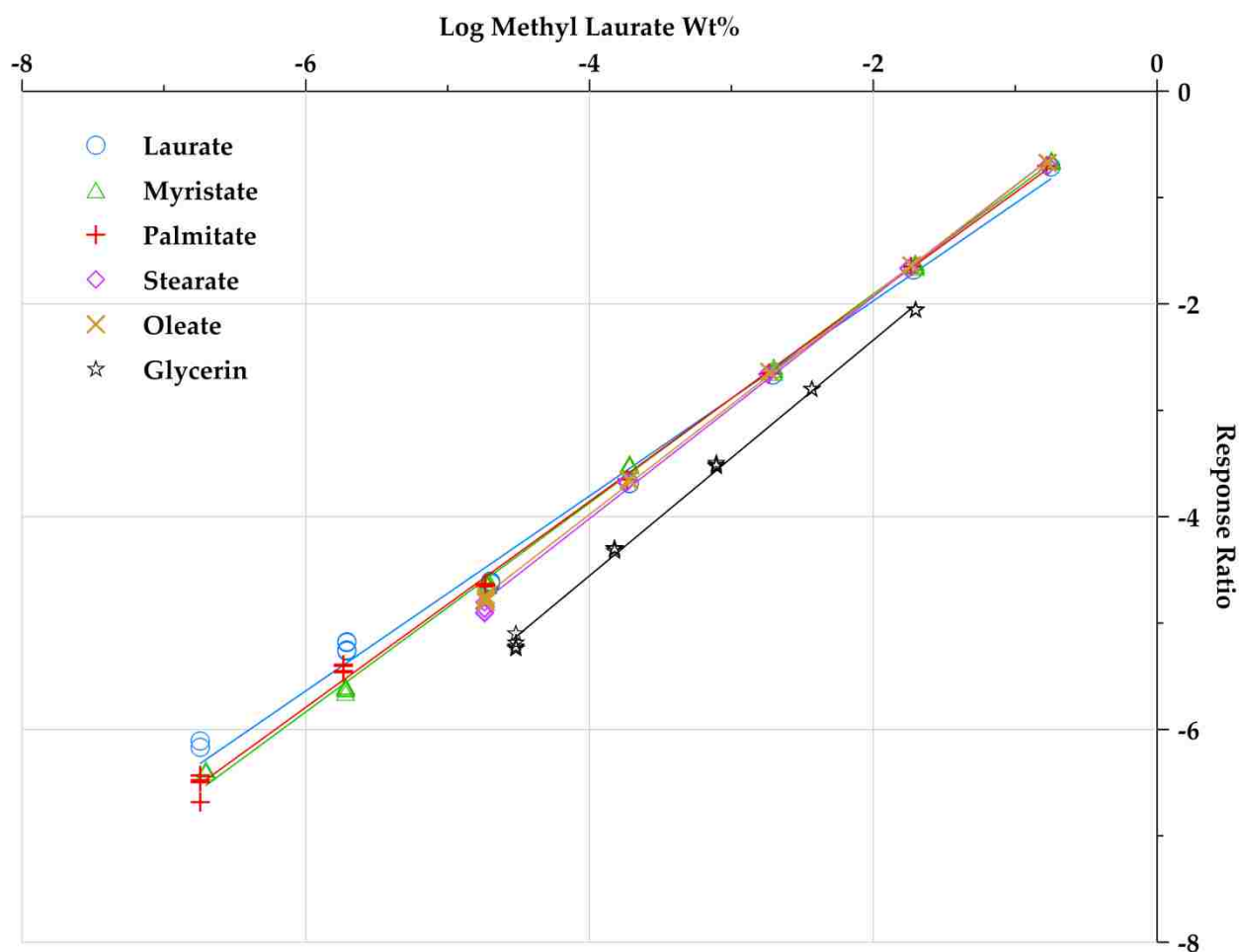
Figure 26: Calibration curves for all five esters and glycerin

While the glycerin curve obviously differs from the rest, the calibrations for the five methyl esters are very similar. While no rigorous tests were performed, it is doubtful there is a statistically significant difference between any of the ester curves; a single curve may have been equally accurate. Because these curves were collected over the course of several months of experimentation, this observation was not made until experiments were nearly complete and was not investigated further.

It has been suggested that response ratios calculated in the manner they were here are a function of the instrument parameters much more than a function of the chemicals being analyzed[45]. The esters were all analyzed with the same instrumental method (heavy phase method, Table 6) while glycerin was analyzed with a different method (light phase method, Table 6). Keeping this in mind, these results reinforce the suggestion that the response ratio is a stronger function of instrument parameters than analyte. There are significant differences in thermophysical properties across the group of esters analyzed, and yet they all line up on nearly identical response ratio curves.

This plot also shows something about the stability of the response ratio method. Raw peak areas from the GC can vary greatly with ambient temperature, pressure, and humidity resulting in significant changes from day to day. Degradation of the active phase in the GC column also leads to significant long term variation. The fact that these points were collected over a six month time period and all lie essentially on the same

line is evidence that the response ratio method does indeed eliminate much of the

inherent variability present in GC analysis.

A.2   Extended Data Tables with Individual Errors

Table 19: Individual error data: Methyl Laurate (x_1) – Water (x_2) – Glycerin (x_3)

Ester Phase					Water/Glycerin Phase				
x_1 (calc)	x_2	$\pm u_2$	x_3	$\pm u_3$	x_1	$\pm u_1$	x_2	$\pm u_2$	x_3 (calc)
0.9958	0.0003	25%	0.0039	2%	2.4x10-5	10%	0.0025	9%	0.9974
0.9918	0.0045	10%	0.0037	17%	2.1x10-5	32%	0.1166	1%	0.8833
0.9891	0.0077	2%	0.0032	9%	1.5x10-5	16%	0.2168	0.4%	0.7832
0.9850	0.0122	3%	0.0029	12%	1.1x10-5	51%	0.3162	1%	0.6838
0.9774	0.0204	1%	0.0023	18%	7.0x10-6	13%	0.5052	2%	0.4948
0.9667	0.0320	2%	0.0013	22%	2.6x10-6	29%	0.7253	1%	0.2747
0.9573	0.0423	1%	0.0004	52%	2.1x10-7	46%	0.8892	1%	0.1108
0.9515	0.0485	0.3%	0.0000	0.0%	2.5x10-7	53%	1.0000	0.0%	0.0000

Table 20: Individual error data: Methyl Myristate (x_1) – Water (x_2) – Glycerin (x_3)

Ester Phase					Water/Glycerin Phase				
x_1 (calc)	x_2	$\pm u_2$	x_3	$\pm u_3$	x_1	$\pm u_1$	x_2	$\pm u_2$	x_3 (calc)
0.9960	0.0011	28%	0.0029	10%	8.3x10-6	62%	0.0024	10%	0.9976
0.9935	0.0041	12%	0.0025	10%	6.8x10-6	10%	0.1163	1%	0.8837
0.9904	0.0072	3%	0.0024	13%	4.7x10-6	44%	0.2099	1%	0.7901
0.9869	0.0110	6%	0.0021	8%	3.3x10-6	63%	0.3166	1%	0.6834
0.9799	0.0184	2%	0.0017	16%	9.6x10-7	38%	0.5055	1%	0.4945
0.9706	0.0286	2%	0.0008	34%	2.9x10-7	83%	0.7232	2%	0.2768
0.9635	0.0363	1%	0.0002	87%	< 1x10-7	---	0.8883	3%	0.1117
0.9579	0.0421	3%	0.0000	0.0%	< 1x10-7	---	1.0000	0.0%	0.0000

Table 21: Individual error data: Methyl Palmitate (x_1) – Water (x_2) – Glycerin (x_3)

Ester Phase					Water/Glycerin Phase				
x_1 (calc)	x_2	$\pm u_2$	x_3	$\pm u_3$	x_1	$\pm u_1$	x_2	$\pm u_2$	x_3 (calc)
0.9960	0.0010	39%	0.0031	25%	8.5x10-6	35%	0.0033	10%	0.9967
0.9933	0.0038	9%	0.0029	12%	4.5x10-6	12%	0.1141	2%	0.8859
0.9906	0.0066	5%	0.0028	19%	1.7x10-6	75%	0.2088	1%	0.7912
0.9873	0.0103	2%	0.0025	46%	1.4x10-6	85%	0.3133	2%	0.6867
0.9803	0.0179	1%	0.0018	34%	8.4x10-7	44%	0.5066	6%	0.4934
0.9697	0.0293	15%	0.0010	68%	< 1x10-7	---	0.7869	3%	0.2131
0.9608	0.0392	1%	0.0000	0%	< 1x10-7	---	0.9531	5%	0.0469

Table 22: Individual error data: Methyl Stearate (x_1) – Water (x_2) – Glycerin (x_3)

Ester Phase					Water/Glycerin Phase				
x_1 (calc)	x_2	$\pm u_2$	x_3	$\pm u_3$	x_1	$\pm u_1$	x_2	$\pm u_2$	x_3 (calc)
0.9913	0.0029	36%	0.0058	46%	2.6x10-6	71%	0.0809	2%	0.9191
0.9890	0.0062	16%	0.0048	77%	1.9x10-6	32%	0.2084	1%	0.7916
0.9843	0.0096	3%	0.0060	16%	1.3x10-6	45%	0.3141	1%	0.6859
0.9802	0.0168	2%	0.0031	35%	< 1x10-6	---	0.5021	2%	0.4979

Table 23: Individual error data: Methyl Oleate (x_1) – Water (x_2) – Glycerin (x_3)

Ester Phase					Water/Glycerin Phase				
x_1 (calc)	x_2	$\pm u_2$	x_3	$\pm u_3$	x_1	$\pm u_1$	x_2	$\pm u_2$	x_3 (calc)
0.9953	0.0006	44%	0.0042	16%	9.2x10-6	109%	0.0028	9%	0.9972
0.9930	0.0036	22%	0.0034	20%	6.1x10-6	177%	0.0825	1%	0.9175
0.9893	0.0077	7%	0.0030	13%	6.3x10-6	18%	0.2169	1%	0.7831
0.9862	0.0110	10%	0.0028	23%	< 1x10-6	---	0.3166	2%	0.6834
0.9814	0.0166	2%	0.0020	12%	< 1x10-6	---	0.5090	2%	0.4910
0.9692	0.0295	1%	0.0013	25%	< 1x10-6	---	0.7276	2%	0.2724
0.9618	0.0376	1%	0.0005	59%	< 1x10-6	---	0.8954	4%	0.1046
0.9574	0.0426	2%	0.0000	0.0%	< 1x10-6	---	1.0000	0.0%	0.0000

Appendix B – The Untold Story

Much of the time and effort expended on this project and knowledge acquired occurred during the apparatus and method development. This phase of the project is quickly glossed over in 0. Details were omitted because in the interest of the results presented what worked is far more important than what did not. However, a summary of experimental efforts that failed and why may be of some future use and is therefore included here.

B.1   Apparatus Development

B.1.1   Cloud Point Titrations

The initial direction of this research was to measure the binodal curve by cloud point titration. This method was introduced in 0. Titrations are performed by starting with a single phase binary mixture. A third component is then titrated in until the mixture clouds indicating that small bubbles of a second phase have formed. Multiple titrations are performed across the two phase region to resolve the binodal curve. A few tie-lines are then measured by some other means to show the slope of tie-lines through the two phase region.

An apparatus similar to that shown in Figure 2 was prepared for titrations. This

original apparatus (1) had a magnetic stir bar instead of the stir shaft shown in Figure 2.

Apparatus 1 also had a titration tube extending down into the liquid and terminating

near the bottom of the vessel. The titration tube had a fine tip (24 gauge needle) which

allowed liquid to be dispensed in very small drops. Liquid was fed into the vessel

through this tube from a mechanical screw-type volumetric pump. Graduations on the

screw pump combined with the fine tip tubing allowed liquid volumes to be dispensed

ranging from 10 μL to 100 mL with an accuracy of ± 5 μL.

Multiple titrations were performed starting with different binary mixtures of

water and glycerin, methyl laurate being titrated in through the pump. The first

experiments appeared to jump from a single phase to several mL of second lighter

phase instantly appearing without ever passing through a cloud point. Closer

inspection showed that the second (light) phase was present from the addition of the

first drop. It took the addition of numerous drops before they coalesced into a single

phase substantial enough to observe through the mild turbulence; however, if the stirrer

was turned off the first drop was clearly visible. Further experiments showed that even

a single drop given several hours of stirring would not dissolve.

After completing measurements and observing results for the methyl laurate

system as outlined in the main body of this work the difficulties encountered with

cloud point titrations are understandable. The cloud point was never observed because a single 10 μL drop of methyl laurate in the volume of water and glycerin used for trial titrations was already beyond the soluble limit.

B.1.2 Magnetic Stirring

The intention had always been to measure a few tie-lines by sampling an equilibrium two phase mixture with compositions determined by GC. Due to the failed trial experiments, cloud point titration was abandoned as a method for measuring a detailed binodal curve. Since the apparatus was already set up for sampling two phases, the next logical method was to perform more equilibrium experiments. The binodal curve and tie-lines would then be measured simultaneously, with tie-lines throughout the entire two phase region.

The titration tube was removed (apparatus 2) and equilibrium experiments were performed with samples analyzed by GC. These experiments accentuated the in-adequate mixing in the cell, a problem which had been observed to some extent during the titration trials. Glycerin is a highly viscous compound, an issue which appeared throughout every phase of experimentation. The magnetic stirrer was incapable of agitating the heavy phase enough to provide intimate contact between the phases. The maximum maintainable stirring speed provided for a gentle vortex at the meniscus between the two liquid phases and no vortex at the surface of the light phase. If the stirring speed was increased, the magnet was incapable of overcoming the viscosity of

the mixture. The stir bar would lose its connection with the magnetic stir plate and stop stirring.

Multiple variations were explored to overcome this. Starting with a mixture that contained more water than glycerin helped but was an in-adequate solution. Even when the heavy phase was mostly water (80% wt) the viscosity was too high for the magnetic stirrer. Numerous measurements were made to determine if stirring at a slower speed for longer periods of time would allow the phases to equilibrate. Mixing times ranging from 15 minutes to several weeks were investigated. The hope was that after some length of mixing the composition would stop changing; however even after three weeks of stirring this was not observed. It became clear that an alternate mixing method was required

B.1.3 High Temperature Mixing

The viscosity of the mixture decreased significantly with increasing temperature, enabling more thorough mixing. Trial experiments were performed varying the temperature over a range of 60 to 90 °C during mixing. At temperatures above 80 °C complete mixing was attainable. The liquid appeared as a homogenous mixture consisting of small globules of each phase.

The phases were then allowed to cool to the desired experimental temperature of 60 °C. Upon cooling the temperature dependence of the equilibrium position was

immediately apparent. Adequate time was allowed for the phases to return to a clear

state after the temperature had equilibrated. This was generally accomplished within

24 hours, after which samples were taken and analyzed.

This method provided reproducible results. After a relatively short length of

mixing time at high temperature (15 minutes) there was no change in composition so

long as the phases were allowed adequate time to return to a clear state at 60 °C before

samples were extracted. GC results from experiments performed with this method

showed numerous peaks that appeared neither in pure component analyses nor in any

previous experiments. The peaks were consistent and represented a significant

percentage of the total peak area: they were far too substantial to be considered noise.

While the most likely explanation may be thermal degradation products of the methyl

ester, the exact nature and source of the peaks was not investigated.

B.1.4 Direct Mechanical Agitation

Having exhausted alternative ways to use the magnetic stirring, apparatus 3

shown in Figure 2 was devised. A pass through compression fitting which seals around

the spinning shaft was designed with the aid of a technical expert at Ace Glass and

constructed in house with parts provided by Ace Glass.

Initial trials using the pass-through stir shaft were not successful. The variable

speed motor in use did not provide adequate torque at the low RPM desired to

overcome friction in the compression fitting. At higher RPM there was sufficient torque; however, the shaft generated excessive heat in the compression fitting destroying the O-rings. The high-torque low-RPM motor described in section 4.1 was obtained as a solution to this issue.

Experiments using apparatus 3 immediately showed thorough mixing of the two phases. The liquid appeared as a very homogenous mixture, small globules of each phase were almost indistinguishable immediately after stirring. The analytical results quickly showed that this direct stirrer provided repeatability none of the previous apparatuses had. Analysis of variance showed five repeated experiments gave the same results at a 95% confidence level and apparatus development was considered complete.

B.2 Method Development

The bulk of the method development occurred during the magnetic stirring phase of apparatus development described in section B.1.2. It was apparent that some variability in the results was due to the method and not the apparatus. Ensuring the method was providing repeatable results was necessary before determining adequacy of the apparatus.

B.2.1   Sample Size and Preparation

Initially small samples were extracted and prepared for analysis. A few drops of sample extracted from the cell were used to prepare small vials for GC analysis. The sample mass used was 10-20 mg with a final prepared sample volume of approximately 1 mL. Samples were prepared in small volumes to conserve chemicals and limit waste. Concentrations of analyte in the prepared solution were kept low to prevent saturating the GC column. Results obtained by this method were extremely scattered with standard deviations of repeated preparations using the same extracted sample on the order of 600%

An internal standardization method was the first attempt at correcting this. Small samples were prepared in the same way just described with a few drops of internal standard added to the solution. Again the mass of internal standard added was 10-20 mg. Response ratios were calculated as described in Equation 6. This reduced the standard deviation of repeated preparations from the same sample to around 300%, still unacceptably large.

It was eventually suggested that larger sample sizes and larger volumes of prepared solution be used. The accuracy of the balance used was ±1 mg. With a 10 mg mass the error introduced by the accuracy of the balance was at least 10%, while a larger mass of 1 g would only contain 0.001% error. Solutions were prepared using larger sample sizes and larger amounts of internal standard as explained in section 4.2.5. This

sample preparation resulted in a much more concentrated solution. Significant

modifications to the GC method were required to accommodate this change and are

discussed in section B.2.2. The results of larger samples were drastic. Repeated

preparations from the same sample now showed a standard deviation of less than 1%.

A similar sample size phenomenon was observed with the Karl-Fischer titration.

The apparatus was calibrated and produced high precision and accuracy using the

calibration standard (water) delivered through a micro-liter syringe. Small sample sizes

of 0.2-0.4 mL of each phase were analyzed for water content. The heavy phase samples

proved very repeatable (standard deviation <1%) while the light phase samples showed

more scatter (standard deviation 20-30%). The amount of water in the light phase was

so small that the error of the instrument (±0.001 mg) was a significant fraction of the

amount of water being titrated in each sample. The light phase sample size was

increased to 3 mL and the standard deviation of repeated samples dropped to <1%.

B.2.2 GC Method – Glycerin Woes

The most significant issue related to glycerin was developing an appropriate GC

method. The high viscosity of glycerin coupled with its relatively high boiling point

(290 °C) made it very difficult to analyze. In order to prevent a slug of liquid glycerin

from entering the column the GC inlet had to be maintained at 350 °C as noted in Table

6. The septum through which samples are injected degraded rapidly because of this

high temperature and had to be replaced at least after every set of six samples. If the septum was not replaced it leaked causing inconsistent results.

Achieving good separation of glycerin in the GC column was difficult. Most compounds elute from a GC column in a very sharp peak over a time span of 1 to 2 seconds. Large concentrations of glycerin would elute over the course of one or two minutes. Obtaining reproducible results with such a broad flat peak is impossible. Further complicating the issue was the fact that this broad plateau overlapped the internal standard and methyl ester peaks.

One potential solution to obtaining a sharp narrow peak was to saturate the carrier gas with water vapor. This can occupy all of the polar sites in the active phase resulting in narrower peaks for polar compounds and slightly shorter retention times, even in a non-polar column. Analyses were performed by bubbling carrier gas through a trap partially filled with water. A second empty trap was installed downstream to knock out any entrained droplets and allow only water vapor to pass through with the carrier gas. Results with water saturated carrier gas were very good. The glycerin peak was much shorter, eluting over about 6-8 seconds.

After several days of operating in this manner, the GC suddenly stopped working entirely. Several weeks of troubleshooting with the aid of online and phone technical support ensued. This was followed by several more weeks with a service

technician on site attempting to diagnose and repair the instrument. The eventual

diagnosis was a malfunctioning section of the gas flow path: a micro-fluidics chip. The

micro-fluidics channels in the chip had become saturated with condensed water and the

gas flow was incapable of forcing the liquid out. Saturating the carrier gas with water

vapor was no longer a viable option.

Prior to this point GC methods had been employing lower split ratios in the

range of 5-10:1. Trials investigating higher split ratios showed potential. The effects of

other GC parameters were also investigated. It was during this time that the peak

broadening and difficulties associated with correcting it discussed in section 5.2 were

observed. The idea of using a different internal standard for each compound also

discussed in section 5.2 did not surface until much later.

It was during this stage the decision was made to use different methods for the

light and heavy phases, as separate methods solved some of the peak broadening

issues. At this point the determination was made *not* to find concentrations of the major

components by GC analysis, but to calculate the concentration by difference. This was

because the glycerin peak with the heavy phase method still did not elute as a sharp

peak but instead as a broad dome. The light phase method allowed small

concentrations of glycerin to be separated from the solvent and internal standard and

elute as a sharp peak; however, the ester peak was not ideal. Measuring minor

82

components with the GC methods outlined in Table 6 while calculating major

components provided an acceptable compromise to the difficult problems posed by the

analysis.

References

(1)   DOE, Annual Energy Review. In *Energy Information Administration*, **2009**; Vol. DOE/EIA-0384(2008).

(2)   Sheehan, J.; Comobreco, V.; Duffield, J.; Graboski, M.; Shapouri, H., Life Cycle Inventory of Biodiesel and Petroleum Diesel for Use in an Urban Bus. In *National Renewable Energy Laboratory*, **1998**; Vol. NREL/SR-580-24089.

(3)   Ilkilic, C., Exhaust emissions of a diesel engine operating by biodiesel fuel. *Energy Sources, Part A* **2009,** *31*, 1415-1424.

(4)   Rickeard, D. J.; Thompson, N. D., A review of the potential for bio-fuels as transportation fuels. *Soc. Automot. Eng., [Spec. Publ.] SP* **1993,** *SP-995*, 109-25.

(5)   Lapuerta, M.; Armas, O.; Rodriguez-Fernandez, J., Effect of biodiesel fuels on diesel engine emissions. *Prog. Energy Combust. Sci.* **2008,** *34*, 198-223.

(6)   Szybist, J. P.; Song, J.; Alam, M.; Boehman, A. L., Biodiesel combustion, emissions and emission control. *Fuel Process. Technol.* **2007,** *88*, 679-691.

(7)   Gaffney, J. S.; Marley, N. A., The impacts of combustion emissions on air quality and climate - From coal to biofuels and beyond. *Atmos. Environ.* **2009,** *43*, 23-36.

(8)   Bazaras, Z.; Kersys, A.; Kersys, R.; Kersiene, N.; Raudys, R. In *Research into the impact of biodiesel usage in transport on sustainable development*, 13th International Conference on Urban Transport and the Environment in the 21st Century, Coimbra, Portugal, WITPress: Coimbra, Portugal, **2007**; pp 503-509.

(9)   Bridgwater, A. V., The production of biofuels and renewable chemicals by fast pyrolysis of biomass. *Int. J. Global Energy Issues* **2007,** *27*, 160-203.

(10)   Williams, P. T.; Horne, P. A., Characterisation of oils from the fluidised bed pyrolysis of biomass with zeolite catalyst upgrading. *Biomass Bioenergy* **1994,** *7*, 223-236.

(11)   Scott, D. S.; Piskorz, J.; Radlein, D., Liquid prosducts from the continuous flash pyrolysis of biomass. *Ind. Eng. Chem. Process Des. Dev.* **1985,** *24*, 581-588.

(12)   Honeywell Envergent Technologies. http://www.envergenttech.com/rtp.php (accessed 11/06/12).

(13)   BTG-BTL Biomass-to-liquid. http://www.btg-btl.com/index.php?r=technology (accessed 11/06/12).

(14)   Digman, B.; Joo, H. S.; Kim, D.-S., Recent progress in gasification/pyrolysis technologies for biomass conversion to energy. *Environ. Prog. Sustainable Energy* **2009,** *28*, 47-51.

(15)   Badger, P. C., Ethanol From Cellulose: A General Review. In *Trends in new crops and new uses*, Janick, J.; Whipkey, A., Eds. **2002;** pp 17-21.

(16)   Lynd, R. L., Overview and evaluation of fuel ethanol from cellulosic biomass: technology, economics, the environment, and policy. Annual Reviews Inc: Palo Alto, CA, United States, **1996;** Vol. 21, pp 403-465.

(17)   Duff, S. J. B.; Murray, W. D., Bioconversion of forest products industry waste cellulosics to fuel ethanol: A review. *Bioresour. Technol.* **1996,** *55*, 1-33.

(18)   Darnoko, D.; Cheryan, M., Kinetics of Palm Oil Transesterification in a Batch Reactor. *J. Am. Oil Chem. Soc.* **2000,** *77* (32), 1263-1267.

(19)   Noureddini, H., Kinetics of Transesterification of Soybean Oil. *J. Am. Oil Chem. Soc.* **1997,** *74* (11), 1457-1463.

(20)   Zhang, Y.; Dube, M. A.; McLean, D. D.; Kates, M., Biodiesel production from waste cooking oil: 1. Process design and technological assessment. *Bioresour. Technol.* **2003,** *89*, 1-16.

(21)   Allen, C. A. W.; Watts, K. C.; Ackman, R. G.; Pegg, M. J., Predicting the viscosity of biodiesel fuels from their fatty acid ester composition. *Fuel* **1999,** *78*, 1319-1326.

(22)   Gao, Y.; Gregor, C.; Liang, Y.; Tang, D.; Tweed, C., Algae biodiesel - a feasibility report. *Chem. Cent. J.* **2012,** *6*, S1.

(23)   Chen, L.; Liu, T.; Zhang, W.; Chen, X.; Wang, J., Biodiesel production from algae oil high in free fatty acids by two-step catalytic conversion. *Bioresour. Technol.* **2012,** *111*, 208-214.

(24)   Schuchardt, U.; Sercheli, R.; Vargas, R. M., Transesterification of Vegetable Oils: A Review. *J. Braz. Chem. Soc* **1998,** *9* (1), 199-210.

(25)   Freedman, B.; Butterfield, R.; Pryde, E. H., Transesterification Kinetics of Soybean Oil. *J. Am. Oil Chem. Soc.* **1986,** *63* (10).

(26)   Freedman, B.; Pryde, E. H.; Mounts, T. L., Variables Affecting the Yields of Fatty Esters from Transesterified Vegetable Oils. *J. Am. Oil Chem. Soc.* **1984,** *61* (10), 1638-1643.

(27)   Goering, C. E.; Schwab, A. W.; Daugherty, M. J.; Pryde, E. H.; Heakin, A. J., Fuel Properties of eleven vegetable oils. *Trans. ASAE* **1982,** *25* (6), 1472-1477.

(28)   Krawczyk, T., Biodiesel. *Int. News Fats, Oils Relat. Mater.* **1996,** *7*, 800-800.

(29)   Noureddini, H.; Harkey, D.; Medikonduru, V., Continuous process for the conversion of vegetable oils into methyl esters of fatty acids. *J. Am. Oil Chem. Soc.* **1998,** *75*, 1775-1783.

(30)   Connemann, J.; Groos, H.; Fischer, J.; Philippsen, A. Method and device for producing biodiesel. US Patent Number 20050204612, **2005**.

(31)   Tizvar, R.; McLean, D. D.; Kates, M.; Dube, M. A., Optimal separation of glycerol and methyl oleate via liquid-liquid extraction. *J. Chem. Eng. Data* **2009,** *54*, 1541-1550.

(32)   Shimoyama, Y.; Iwai, Y.; Abeta, T.; Arai, Y., Measurement and correlation of vapor-liquid equilibria for ethanol + ethyl laurate and ethanol + ethyl myristate systems near critical temperature of ethanol. *Fluid Phase Equilib.* **2008,** *264*, 228-234.

(33)   Shimoyama, Y.; Iwai, Y.; Jin, B. S.; Hirayama, T.; Arai, Y., Measurement and correlation of vapor-liquid equilibria for methanol + methyl laurate and methanol + methyl myristate systems near critical temperature of methanol. *Fluid Phase Equilib.* **2007,** *257*, 217-222.

(34)   Bonhorst, C. W.; Althouse, P. M.; Triebold, H. O., Esters of Naturally Occuring Fatty Acids. *Ind. Eng. Chem.* **1948,** *40* (12), 2379-84.

(35)   Andreatta, A. E.; Casas, L. M.; Hegel, P.; Bottini, S. B.; Brignole, E. A., Phase equilibria in ternary mixtures of methyl oleate, glycerol, and methanol. *Ind. Eng. Chem. Res.* **2008,** *47*, 5157-5164.

(36)   Negi, D. S.; Sobotka, F.; Kimmel, T.; Wozny, G.; Schomacker, R., Liquid-liquid phase equilibrium in glycerol-methanol-methyl oleate and glycerol-monoolein-methyl oleate ternary systems. *Ind. Eng. Chem. Res.* **2006,** *45*, 3693-3696.

(37)   Cehreli, S., Liquid-liquid equilibria of the acetic acid-water-mixed solvent (cyclohexyl acetate-cyclohexanol) system. *Braz. J. Chem. Eng.* **2002,** *19*, 45-53.

(38)   Letcher, T. M.; Siswana, P. M.; Van, d. W. P.; Radloff, S., Phase equilibria for (an alkanol + p-xylene + water) at 298.2 K. *J. Chem. Thermodyn.* **1989,** *21*, 1053-60.

(39)   Ochi, K.; Tada, M.; Kojima, K., Measurement and correlation of liquid-liquid equilibria up to critical solution temperature. *Fluid Phase Equilib.* **1990,** *56*, 341-359.

(40)   Ochi, K.; Kato, Y.; Saito, T.; Kurihara, K.; Kojima, K., Determination and correlation of LLE and SLE data for the system aniline+cyclohexane. *Korean J. Chem. Eng.* **1997,** *14* (5), 365-368.

(41)   Steyer, F.; Sundmacher, K., VLE and LLE data for the system cyclohexane + cyclohexene + water 4 + cyclohexanol. *J. Chem. Eng. Data* **2004,** *49*, 1675-1681.

(42)   Garcia, J.; Fernandez, A.; Torrecilla, J. S.; Oliet, M.; Rodriguez, F., Ternary liquid-liquid equilibria measurement for hexane and benzene with the ionic liquid 1-butyl-3-methylimidazolium methylsulfate at T = (298.2, 313.2, and 328.2) K. *J. Chem. Eng. Data* **2010,** *55*, 258-261.

(43)   Huemer, H.; Woertl, K.; Moser, F., New apparatus for measurement of liquid-liquid equilibrium data, and results for the water-methanol-dichloromethane system at 20 and 60 degrees C. *Fluid Phase Equilib.* **1983,** *11*, 311-323.

(44)   Schoonover, R. M.; Jones, F. E., Air buoyancy correction in high-accuracy weighing on analytical balances. *Anal. Chem. (Washington, DC, U. S.)* **1981,** *53* (6), 900-902.

(45)   Cicchetti, E.; Merle, P.; Chaintreau, A., Quantitation in gas chromatography: Usual practices and performances of a response factor database. *Flavour Fragrance J.* **2008,** *23* (6), 450-459.

(46)   Skoog, D. A.; Holler, F. J.; Crouch, S. R., *Principles of Instrumental Analysis*. Sixth ed.; Thomson Brooks Cole: **2007;** p 1039.

(47)   Vicentim, M. P.; Barreto Sousa, M. V.; Fernandes Da Silva, V.; Lionel Mateus, V.; Rodrigues, J. M.; Smargaro Da Cunha, V., Water content determination in biodiesel: Optimization of methodology in coulometric karl fischer titration. *J. ASTM Int.* **2010,** *7* (2), 1-7.

(48)   Dietrich, A.; Pohmer, J., Karl Fischer titration part 3: quantitative analysis of water in amines and hydrocarbons. *Am. Lab. (Shelton, CT, U. S.)* **1996,** *28* (17), 34-41.

(49)   Miller, J. C.; Miller, J. N., Statistics for Analytical Chemsitry. 2 ed.; Ellis Horwood: Chichester, England, **1988;** pp 109-115.

(50)   Renon, H.; Prausnitz, J. M., Local compositions in thermodynamic excess functions for liquid mixtures. *AIChE J.* **1968,** *14* (1), 135-144.

(51)   Prausnitz, J. M.; Lichtenthaler, R. N.; Gomes de Azevedo, E., Molecular Thermodynamics of Fluid-Phase Equilibria. 3 ed.; Prentice Hall: Upper Saddle River, New Jersey, **1999;** pp 258-294.

(52)   Seader, J. D.; Henley, E. J., Separation Process Principles. 2 ed.; John Wiley & Sons, Inc.: Hoboken, NJ, **2006;** pp 295-313.

(53)   Tizvar, R.; McLean, D. D.; Kates, M.; Dube, M. A., Liquid-liquid equilibria of the methyl oleate-glycerol-hexane-methanol system. *Ind. Eng. Chem. Res.* **2008,** *47*, 443-450.